Modeling and analysis of a three-degree-of-freedom piezoelectric vibration energy harvester for broadening bandwidth

Bin Zhang[a,*], Haoyuan Li[a], Shengxi Zhou[b,*], Jinhui Liang[a], Jun Gao[a], Daniil Yurchenko[c]

[a] School of mechanical, Electrical & Information Engineering, Shandong University, Weihai, 264209, China.

[b] School of Aeronautics, Northwestern Polytechnical University, Xi'an 710072, China.

[c] Institute of Sound and Vibration Research, University of Southampton, Southampton, SO17 1BJ, UK.

*Corresponding Author: zhoushengxi@nwpu.edu.cn (S. Zhou); bin.zhang@sdu.edu.cn (B. Zhang)

Abstract

This study proposes a multi-frequency response piecewise-linear piezoelectric vibration energy harvester (MFRPLP-VEH) by combining the linear multi-frequency resonance and nonlinear vibration bandwidth broadening methods to improve the working frequency bandwidth and environmental robustness of the piezoelectric vibration energy harvester. A theoretical model is established based on the electromechanical coupling and the dynamic response of the MFRPLP-VEH. The energy harvesting performance and broadening width efficiency of the MFRPLP-VEH were obtained through an experimental verification platform. An error rate of 5% is observed between the numerical results of the theoretical model and the experiment results. Furthermore, the operating frequency range is widened by 67.8% at an external excitation acceleration of 10 m/s^2. The energy generated by the MFRPLP-VEH is 194% of the energy generated by its linear counterpart under the same excitation conditions. The numerical and experimental results verify the accuracy of the theoretical model and the broadband working frequency range of the MFRPLP-VEH.

Keywords: Piezoelectric energy harvesting; Electromechanical coupling; Broadband; Nonlinear; Multi-frequency

1. Introduction

Given the increasing applications of low-power consumption sensor networks, reliable energy supply technologies have become a research focus. Chemical batteries, however, have

limited service life, high replacement, and maintenance costs, and are not environmentally friendly. Therefore, there is an urgent need for developing new energy sources that exhibit long service life, compact size, are light weight, and environmental friendly to compensate for the shortcomings of traditional chemical batteries. An alternative energy solution is by converting energy sources such as kinetic energy, thermal energy, light energy, and wind energy collected from the ambient environment into electric energy [1-4]. Therefore, different energy harvesters were designed and tested [5-9]. For example, a piezoelectric vibration energy harvester can power low-energy consumption devices and sensors by converting vibration energy into electricity [10–15]. However, because the natural vibration excitations have relatively low frequency and intensity, the harvester is usually designed to magnify the amplitude [16, 17], speed [18], and frequency [19–21]. Furthermore, the output power is highly dependent on the resonance of the harvester exhibiting external excitation, which is not always constant [22]. Therefore, researchers have proposed multiple designs of energy harvesters to broaden the working frequency range of the piezoelectric vibration energy harvester through theories and experiments [23–25]. The existing methods used to broaden the frequency range of the harvester can be divided into two categories:

One is the linear multi-frequency resonance method, wherein a harvester is designed to have multiple resonant frequencies within the frequency range of the vibration source and generates multiple resonant peaks [26–28]. Ferrari *et al.* [29] proposed a piezoelectric vibrational energy harvester with three cantilever beams arranged in an array structure. The cantilever beams exhibit their own resonant frequency due to their different structures. Once the external vibration source is close to either of the three resonant frequencies, the corresponding Beam Can significantly increase the output power. Dhote *et al.* [30] designed a harvester using multiple multi-mode cantilever beams in the same plane. The cantilever beams exhibited multi-mode characteristics and generated multi-step resonant frequencies to achieve a broadband frequency range. Results showed that due to the linear multi-frequency resonance, the different vibration units effectively expanded the working frequency range by accumulating the working frequency band. Recently, a global device optimization procedure was proposed for an energy harvester comprising an array of beams. While the proposed design was used to increase the

power density and not the bandwidth, it proved to be effective and resulted in a remarkable 0.3 W power output for the gravity-based device [31]. However, the working frequency band was limited around the resonant frequency because the harvester was still linear. Moreover, the working frequency range of a single vibration unit remained unchanged, which increased the volume of the harvester and decreased the output power density.

The second method is the nonlinear frequency-broadening method. Compared with linear harvester, elaborately introduced nonlinearity, such as structural design [32, 33], magnetic force [34, 35] and other methods [36], could increase the operation bandwidth of the energy harvester, which is conducive to energy harvesting. Li *et al*. [37] investigated a nonlinear X-shaped piezoelectric energy harvester with horizontal and vertical installation configurations, which can achieve tunable bandwidth harvesting by adjusting its structural parameters. Internal resonance is explored to enhance vibration-based energy harvesting by Chen *et al* [38]. Under the influence of internal resonances, the amplitude-frequency response curves have two peaks bending to the left and right respectively. As the results, the internal resonance design produces more power than other designs especially under the Gaussian white noise and the exponentially correlated noise. Lu *et al*. [39] designed a bistable piezo-composite plate for both vibration isolation and energy harvesting, predicted analytically the hardening nonlinearity bending of the amplitude–frequency response curves. The results show that the bistable piezo-composite plate improves the feasibility and effectiveness of the integrated design. Magnetic forces have also been used to broaden the frequency to enhance energy harvesting devices [40 – 43]. Zhou *et al.* [44] presented an impact-induced method for nonlinear energy harvesters to obtain high-energy orbits over a wide frequency range under low excitation levels. Results showed that the working bandwidth significantly enhanced the energy-harvesting performance under low excitation levels. Dai *et al*. [45] studied nonlinear modeling and dynamic analysis of cantilever microbeams and explored the effect of the size of material microstructures on the energy harvesting performance. The frequency response curve exhibited clear softening-type behavior under harmonic excitations. In addition, collisional piecewise nonlinearity is also an effective means to improve the performance of the harvester [46, 47]. A piecewise linear design was used to broaden the working frequency range of the energy harvester through collisions between the

vibration components and the limiter, which changes the equivalent stiffness of the harvester to attain the effect of nonlinear characteristics [48, 49]. Peng *et al.* [50] introduced the impact frequency-up conversion effect into stacked piezoelectric energy harvester structures. Compared to the control group without truncation, the average power is enhanced by over 177 times and the matched resistance is significantly reduced from over 5 kΩ to 73.10 Ω. Soliman *et al.* [51] proposed a piecewise-linear magnetic-electric vibration energy harvester by placing a stopper within the vibration range of the cantilever beam. When the amplitude of the piezoelectric cantilever beam is greater than the clearance, a collision occurs between the beam and the retaining block, which changes the equivalent stiffness of the beam in the piecewise linear mode. As a result, the overall performance of the energy harvester was nonlinear. Furthermore, results showed that the piecewise linear method could effectively broaden the operating frequency of the harvester. The above methods can successfully broaden the working frequency range of harvesters and improve the energy harvesting efficiency.

This study proposes the multi-frequency response piecewise-linear piezoelectric vibration energy harvester (MFRPLP-VEH) by combining the linear multi-frequency resonance method and the nonlinear frequency broadening method to further enhance the performance of the piezoelectric vibration energy harvester and its environmental robustness. The three cantilever beams of the MFRPLP-VEH are active and colliding beams, whose coupling effect exhibits nonlinear characteristics. Then a theoretical model is established based on the electromechanical coupling and the dynamic response of the MFRPLP-VEH. All the outputs of the collision beams are carefully considered and modeled. In order to validate the broadband performance and energy harvesting efficiency of the proposed MFRPLP-VEH, an experimental setup is developed. This design expands the working frequency band of the vibration energy harvester and makes it possible to have a continuous and stable output.

2. Modeling

As shown in Figure 1, the proposed MFRPLP-VEH comprises a base structure and three piezoelectric cantilever beams with adjacent resonant frequencies. Each piezoelectric beam is fabricated using piezoelectric patches and structural alloy steel for the substrate layer having the same dimension parameters. The tip masses are different owing to the different resonant

frequencies of the cantilever beams. Table 1 summarizes the dimensions and material parameters of the piezoelectric cantilever beams.

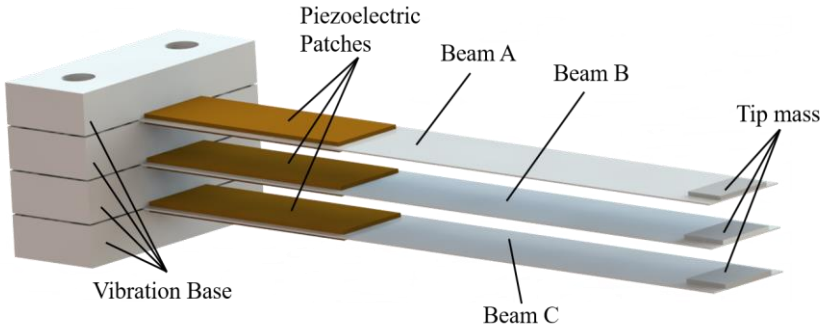

Figure 1 The proposed MFRPLP-VEH.

Table 1 Parameters of the cantilever piezoelectric beams.

Parameter	Value
Beam length	100 mm
Beam width	12 mm
Beam thickness	0.2 mm
Beam density	7900 kg/m^3
Young's modulus of the beam	120 Gpa
The tip mass of Beam A	0.5 gram
The tip mass of Beam B	0 gram
The tip mass of Beam C	0.3 gram
PZT length	30 mm
PZT width	10 mm
PZT thickness	0.4 mm
PZT density	7600 kg/m^3
Piezoelectric capacitance	26.5 nF
Piezoelectric constant	150×10^{-12} m/V
Permittivity of the PZT	1800
Young's modulus of the PZT	80 Gpa

The vibration exciter drives the cantilever beam to vibrate vertically to generate a bending moment, and the piezoelectric patches convert the mechanical vibration energy into electricity.

Once the relative displacement of the two piezoelectric beams is greater than the gap, the beams collide. During periodic motion, the collision causes the stiffness to be nonlinear. The three double-crystal piezoelectric beams are denoted as beams A, B, and C, from top to bottom, and have resonant frequencies of $f_A<f_C<f_B$, respectively. When the frequency sweeps from low to high, Beam A resonates first. When the amplitude of vibration exceeds gap d_1 between beams A and B, they begin to collide. As the excitation frequencies increase, Beam A breaks out of resonance, and its amplitude gradually decreases with no collision. The amplitude of Beam C gradually increases, and it begins to resonate. When the amplitude of vibration exceeds gap d_2 between beams B and C, they begin to collide. As the excitation frequencies increase further, Beam C breaks out of resonance while Beam B continues to resonate and collide with the other two beams.

Giving that the dynamic behavior of mechanical collisions is very complex, the exact results of the vibration response are rarely obtained. Therefore, a variety of average or approximate methods have been developed to give the nonlinear solution [52, 53]. The MFRPLP-VEH is theoretically analyzed by combining the equivalent spring-mass-damping model with piecewise linear springs. Furthermore, to analyze the energy harvesting performance of each beam individually, the damping of the resonant beam is considered, whereas the damping of the non-resonant beams is disregarded [54]. Then, modeling analysis was performed for beams A, B, and C. Figure 2 shows the schematic model of the MFRPLP-VEH.

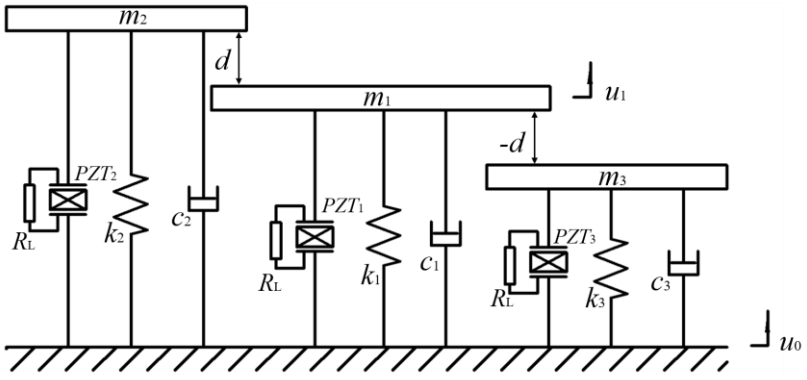

Figure 2 Schematic model of the MFRPLP-VEH.

As shown in Figure 2, subscripts 1, 2 and 3 refer to beams A, B, and C, respectively. We consider the collision of any two beams for analysis. m_1 is the equivalent vibration mass. k_1 is the equivalent stiffness, and c_1 is the equivalent damping of the resonant beam. m_2 (m_3), k_2 (k_3),

and c_2(c_3) are the equivalent mass, stiffness, and damping of the impact beams, respectively. PZTs ($_{1\text{-}2\text{-}3}$) are piezoceramics bonded to beams A, B, and C, respectively. $u_0(t)$ and $u_1(t)$ represent the external excitation and displacement of the resonant beam, respectively. The motion of the resonant beam can be classified into free vibration motion and collision motion. The stiffness and damping of the resonant beam remain unchanged when the relative displacement u_1-u_0 is smaller than the clearance d and change when the two cantilever beams collide. Note that the collision time is kept short for the convenience of the theoretical modeling and analysis [55, 56] and the pre-impact momentums of the beams are small. Furthermore, the speed of the two beams after the collision is assumed to be the same, and the collision beams obey the conservation law of momentum. In other words, the collision is completely inelastic. Based on these assumptions, the stiffness and damping of the two beams would be connected in parallel. The corresponding nonlinear motion equation is given as:

$$m(\ddot{y}+\ddot{y}_0)+c_1\dot{y}+k_1y+f(\dot{y},y)+F_p=0 \tag{1}$$

Herein, y_0=u_0(t)=Ucos(ωt), where U and ω represent the excitation amplitude and excitation frequency, respectively. $f(\dot{y},y)$ in Eq. (1) represents the nonlinear term of the MFRPLP-VEH and is given as:

$$f(\dot{y},y)=\begin{cases} c_1\dot{y}+k_1(y+d) & (y>d) \\ 0 & (y\le d) \end{cases}$$

Because the mechanical model ignores the electromechanical coupling, a significant error was observed between the theoretical derivation and experimental results. Therefore, piezoelectric damping caused by the external load could improve the model accuracy.

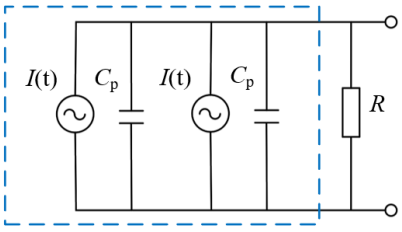

Figure 3 Equivalent circuit of a piezoelectric beam (with two piezoelectric patches connected in parallel).

$I_{up}(t)$ and $I_{down}(t)$ are the two piezoelectric patches pasted on both sides of the piezoelectric beam. Figure 3 shows the bimorph equivalent circuit. The total equivalent capacitance C_p and

current $I(t)$ (sum of I_{up} and I_{down}) of the bimorph piezoelectric cantilever beam are given as:

$$C_{\mathrm{p}} = \frac{L_{\mathrm{p}} W_{\mathrm{p}} \varepsilon_{\mathrm{p}}}{2T_{\mathrm{p}}} \tag{2}$$

$$I(t) = -\Theta \dot{y} \tag{3}$$

According to Kirchhoff's law, the governing equation of the circuit is obtained as:

$$C_{\mathrm{p}} \dot{v} + v / R = \Theta \dot{y} \tag{4}$$

where L_{p}, W_{p}, and T_{p} in Equation (2) represent the length, width, and thickness of the piezoelectric patch, respectively, and ε_{p} is the dielectric constant of the piezoelectric material. In Equation (4), Θ is the electromechanical coupling coefficient, and v is the open-circuit voltage at both ends of the piezoelectric patch.

Therefore, the nonlinear governing equations are given as:

$$\begin{cases} m(\ddot{y} + \ddot{y}_0) + c_1 \dot{y} + k_1 y + f(\dot{y}, y) + F_{\mathrm{p}} = 0 \\ C_{\mathrm{p}} \dot{v} + v / R = \Theta \dot{y} \end{cases} \tag{5}$$

3. Dynamic analysis

The nonlinear differential equation of the MFRPLP-VEH has been described in the previous section. Furthermore, the asymptotic method (average method) is adopted to solve the set of coupled equations of motion. To better understand the theoretical model, we derive the following equation from Equation (5):

$$\begin{cases} \ddot{y}_0 + \dfrac{c_1}{m} \dot{y} + \dfrac{\Theta V(t)}{m} + \dfrac{1}{m} f(\dot{y}, y) = -\ddot{y} - \dfrac{k_1}{m} y \\ \dot{V}(t) + \dfrac{1}{RC_p} V(t) - \dfrac{\Theta}{C_p} \dot{y} = 0 \end{cases} \tag{6}$$

The left side of the first equation is the external excitation term, where $\ddot{y}_0$, mechanical damping, $\frac{c_1}{m}\dot{y}$, piezoelectric damping term, and $f(\dot{y}, y)$ is the nonlinear term. In the occurrence of a nonlinear vibration collision, the terms on the left have less influence on the vibration response than the linear terms on the right, which can be temporarily ignored. Therefore, a new parameter B_{p} is introduced, which represents the sum of the four terms on the left, and ε is used as the prefix to indicate an infinitesimal quantity. Therefore, Equation (6) can be further simplified as:

$$\begin{cases} \varepsilon B_{\mathrm{p}} = -\ddot{y} - x_1 y \\ \dot{V}(t) - x_2 \dot{y} + x_3 V(t) = 0 \end{cases} \tag{7}$$

where the newly introduced parameters x_1, x_2, x_3 are given as:

$$x_1 = \frac{k_1}{m},\ x_2 = \frac{\Theta}{C_{\mathrm{p}}},\ x_3 = \frac{1}{RC_{\mathrm{p}}}, \tag{8}$$

and B_{p} is given as:

$$B_{\mathrm{p}} = \ddot{y}_0 + \frac{c_1}{m}\dot{y} + \frac{1}{m} f(\dot{y}, y) + \frac{\Theta}{m} V(t) \tag{9}$$

After introducing $\varepsilon B_{\mathrm{p}}$, Equation (6) can be further simplified to solve the collision energy harvesting motion, as

$$\begin{cases} \ddot{y} + x_1 y = 0 \\ \dot{V}(t) - x_2 \dot{y} + x_3 V(t) = 0 \end{cases} \tag{10}$$

By solving Equation (10), we obtain the solution of Equation (5) as:

$$\begin{cases} y = D\cos\theta \\ \dot{y} = -\omega_n D\sin\theta \\ V(t) = \left(\dfrac{\omega_n^2 x_2}{\omega_n^2 + x_3^2}\cos\theta - \dfrac{\omega_n x_2 x_3}{\omega_n^2 + x_3^2}\sin\theta \right) D \\ \theta = \omega t + \varphi \\ \omega_n = \sqrt{x_1} \end{cases} \tag{11}$$

where D is the amplitude of the system displacement y, θ is the phase angle of y, ω_n corresponds to the natural frequency of the linear system, and φ is the phase difference between θ and the phase angle of the external excitation. The nonlinear part of the MFRPLP-VEH can be solved by eliminating the infinitesimal quantity ε after the linear system solution is obtained.

The displacement amplitude D is given as:

$$D = \frac{A_0 \omega^2}{\sqrt{\left(\lambda^2(D) - \omega^2\right)^2 + 4\delta^2(D)\omega^2}} \tag{12}$$

The phase difference φ is given as:

$$\varphi = \tan^{-1}\left[-\frac{2\delta(D)\omega}{\lambda^2(D) - \omega^2} \right] \tag{13}$$

The coefficient $\delta(D)$ of the nonlinear amplitude function is given as:

$$\delta(D) = \frac{c_1}{2m} - \frac{\Theta x_2 x_3}{2m\left(\omega_n^2 + x_3^2\right)} - \frac{c_2}{2\pi m} G \tag{14}$$

The equivalent natural frequency $\lambda(D)$ of the MFRPLP-VEH is given as:

$$\lambda(D) = \omega_n + \frac{\Theta \omega_n x_2}{2m\left(\omega_n^2 + x_3^2\right)} - \frac{k_2}{2\pi\omega_n m} G \tag{15}$$

To plot the amplitude-frequency curve, ω is derived from Equation (12) as:

$$\omega = \sqrt{\frac{\left(\lambda^2 - 2\delta^2(D)\right) \pm \sqrt{\left(\lambda^2 - 2\delta^2(D)\right)^2 - \left(1-h^2\right)\lambda^4(D)}}{1-h^2}} \tag{16}$$

where $h = A_0 / D$ is the displacement amplitude ratio between the external excitation and the MFRPLP-VEH.

When continuous amplitude D is known, $\delta(D)$ and $\lambda(D)$ can be calculated by substituting Equations (14) and (15) in Equation (16) to obtain the corresponding value of ω. According to Equation (11), the relationship between the output voltage and displacement of the energy collection system can be deduced as:

$$\begin{aligned} V &= \frac{\omega_n x_2}{\sqrt{\omega_n^2 + x_3^2}} D \\ \theta_1 &= \theta + \varphi_1 \end{aligned} \tag{17}$$

where the phase difference ϕ_1 is given as:

$$\varphi_1 = \tan^{-1} \frac{x_3}{\omega_n} \tag{18}$$

To obtain the relationship between the output voltage V and external excitation frequency ω, we set $\gamma = \frac{\sqrt{\omega_n^2 + x_3^2}}{\omega_n x_2}$ and substitute Equation (17) into Equation (16) as:

$$\omega = \sqrt{\frac{\left(\omega_n^2 - 2\delta^2(D)\right) \pm \sqrt{\left(\omega_n^2 - 2\delta^2(D)\right)^2 - \left(1 - \left(\frac{A_0}{\gamma V}\right)^2\right)\lambda^4(D)}}{1 - \left(\frac{A_0}{\gamma V}\right)^2}} \tag{19}$$

The piezoelectric patches are considered as a current source containing internal resistance:

$$R_{\mathrm{p}} = \frac{1}{2\pi f C_{\mathrm{p}}} \tag{20}$$

Therefore, the output power of the MFRPLP-VEH can be obtained as:

$$P = \frac{V^2 R}{(R_p + R)^2} \tag{21}$$

Beam A is used as an example to explain the working principle of the collision. As shown in Figure 4, the simulation was carried out using Equation (19), and the parameters are listed in Table 1.

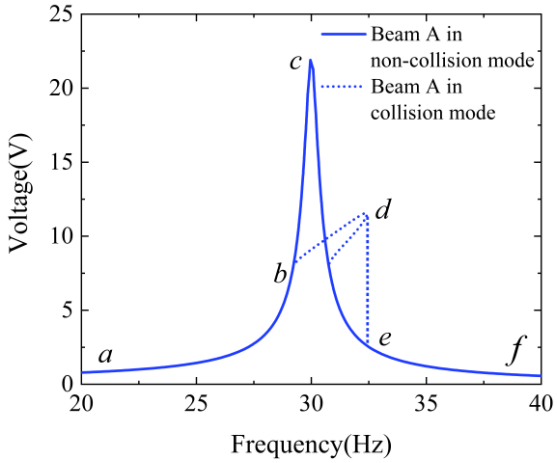

Figure 4 Voltage-frequency characteristic curve of Beam A (at excitation acceleration of 10 m/s^2).

The collision clearance between beams A and B was set to 5 mm. As the excitation frequency gradually increased, the output voltage of Beam A increased from point *a* to point *b*. When the excitation frequency reaches point *b*, the relative displacements of beams A and B become larger than the clearance *d*, and a collision occurs. As a result, the voltage amplitude-frequency curve of Beam A starts to deflate from point *b* to point *d* and is no longer the same as that of the original linear system (solid line). On reaching point *d*, the amplitude drops directly from point *d* to the corresponding amplitude of the linear system at point *e*. The amplitude continues to decline along the linear amplitude-frequency curve.

Similarly, we can obtain the voltage amplitude-frequency curve based on the simulations of the voltage amplitude-frequency curve when the three beams collide with each other in turns, as shown in Figure 5. For example, when Beam B starts to resonate at approximately 40 Hz, it collides with beams A and C considering the clearances are the same. Both the resonant and collision beams generate electricity. The effective working bandwidth can be broadened significantly to enhance the vibration energy under a large bandwidth variation.

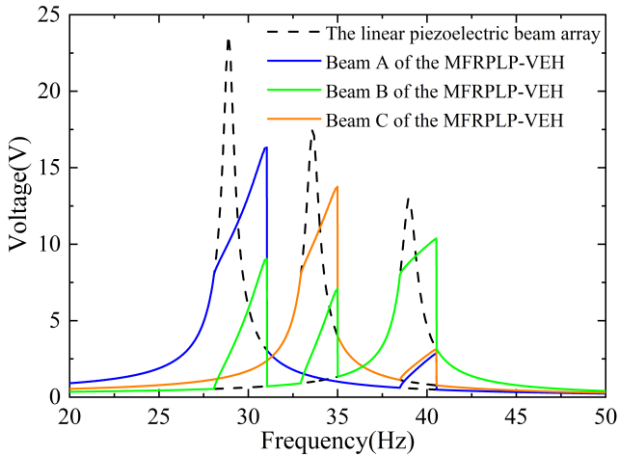

Figure 5 Numerical voltage amplitude-frequency curves of the MFRPLP-VEH and the linear piezoelectric beam array.

4. Experiments and discussion

To verify the three-dimensional model structure of the MFRPLP-VEH, three bimorph cantilever beams with adjacent resonant frequencies are fabricated, as shown in Figure 6. Two piezoelectric patches are bonded in a parallel connection in the opposite polarization directions. The parameters of the fabricated MFRPLP-VEH are listed in Table 1.

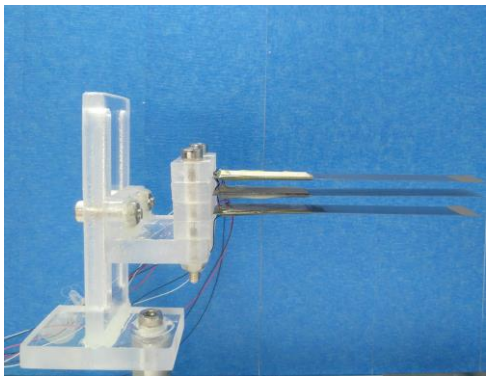

Figure 6 The MFRPLP-VEH in experiment.

Figure 7 shows the experimental setup, which is comprised an arbitrary function generator (Tektronix-AFG1062), power amplifier (YE5874A), shaker (JZK-50), digital oscilloscope (Rohde & Schwarz RTB2004), laser vibrometer (Keyence LK-GD500), and a noise current preamplifier (SR570-Low). A frequency-swept signal is generated by the function generator to control the power amplifier, which in turn is connected to the shaker. An accelerometer is used to monitor the output acceleration. The current and voltage of the MFRPLP-VEH are measured using a current amplifier and an oscilloscope.

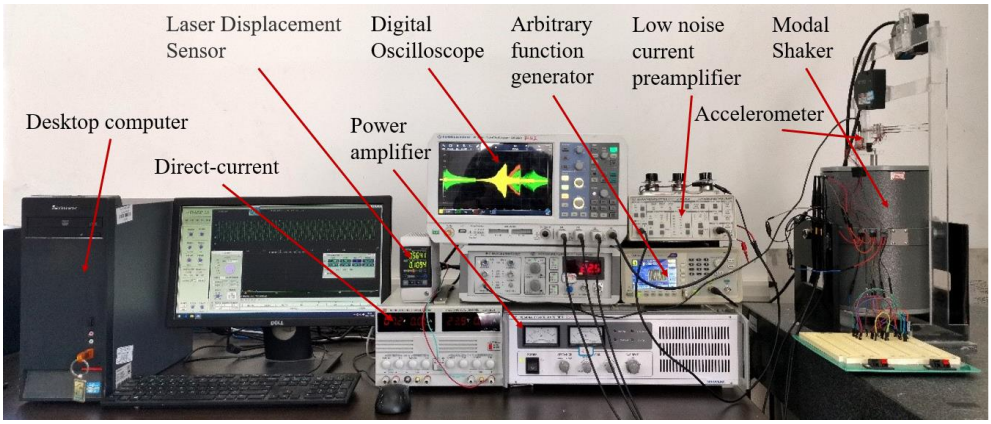

(a)

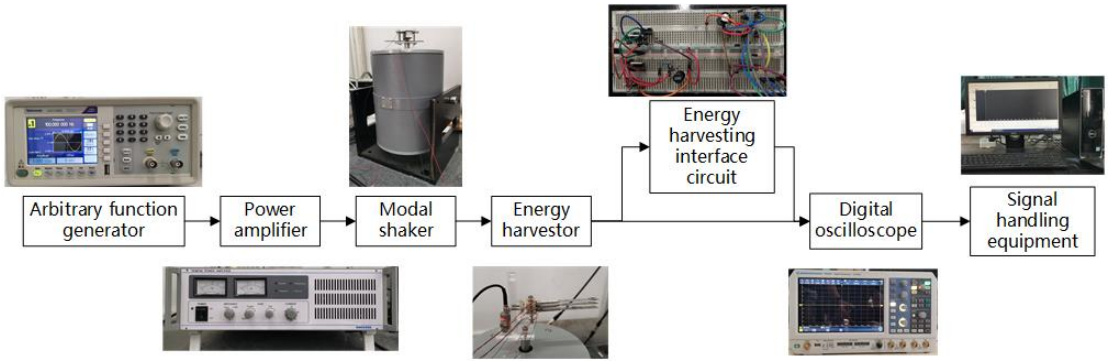

(b)

Figure 7 (a) Experimental setup; (b) flow diagram with experimental devices.

4.1 Output and bandwidth broadening experiment

First, the voltages of the piezoelectric beams are recorded by exciting the beams individually under a constant acceleration of 10 m/s^2 (frequency sweeping from 20 Hz to 50 Hz, sweeping time of 200 s), as shown in Figure 8. As the excitation acceleration remained unchanged, the peak value of the voltage decreased, and the frequency increased. The free vibration mode measurements are in good agreement with the simulations shown in Figure 5. The resonant frequencies of beams A, B, and C in experiment are calculated as 28.9, 33.6, and 38.6 Hz, respectively.

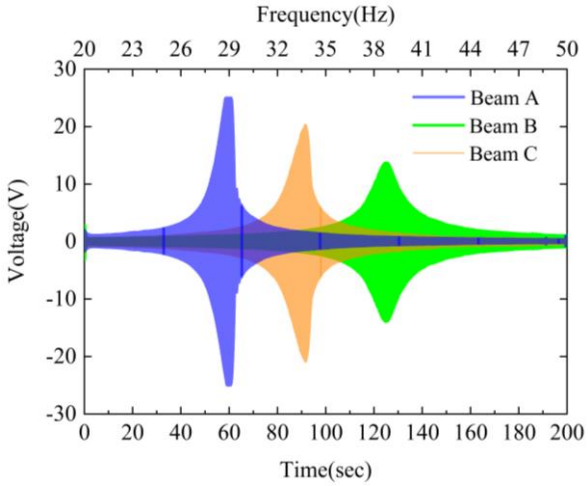

Figure 8 Individual tests (non-collision) of the frequency-swept voltage response curves of each beam under a constant acceleration of 10 m/s^2 (frequency sweeping from 20 Hz to 50 Hz, sweeping time of 200 s).

Impedance matching is performed for each piezoelectric beam at their corresponding resonant frequencies. The output voltage and output power curves, along with the external load impedance, can be obtained, as shown in Figure 9.

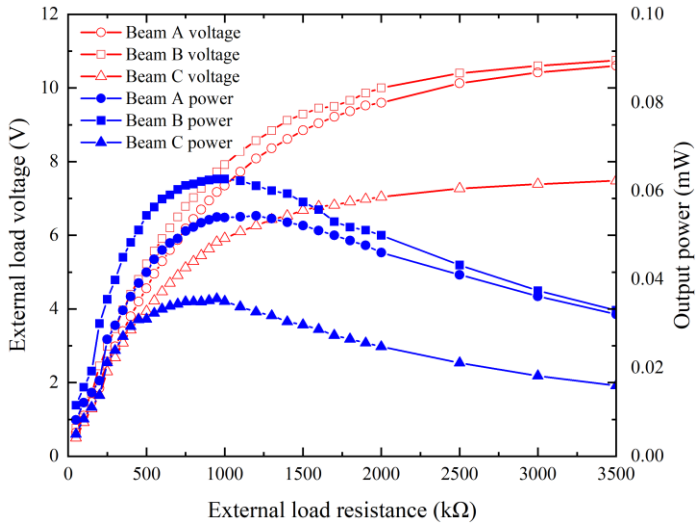

Figure 9 Non-collision output voltage and power curve versus the external load impedance of the MFRPLP-VEH.

As shown in Figure 9, as the external load impedance increases, the output voltage gradually increases until it converges with the open-circuit voltage of the harvester. Simultaneously, the maximum output power of each piezoelectric beam increases as the external load impedance increases. When the external load impedance reaches a peak value, the maximum output power decreases gradually. Then, we conducted the frequency-swept collision experiments at 8 m/s^2,

10 m/s^2, 12 m/s^2, and 14 m/s^2 with the same frequency-swept setting. The experimental results are shown in Figure 10.

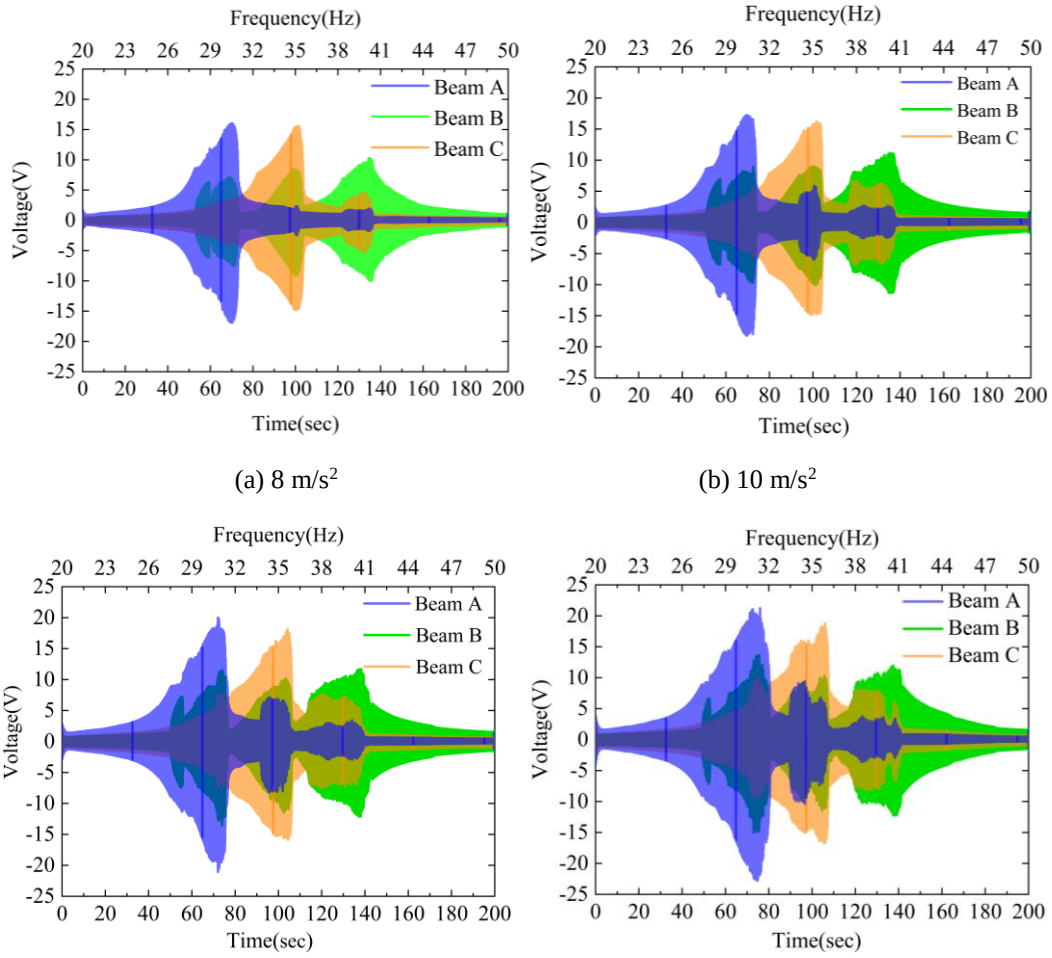

(a) 8 m/s^2 (b) 10 m/s^2

(c) 12 m/s^2 (d) 14 m/s^2

Figure 10 The frequency-swept voltage response curve of MFRPLP-VEH under different acceleration excitations (the frequency sweeping from 20 Hz to 50 Hz, the sweeping time of 200s).

The numerical and experimental results are compared to verify the theoretical model. Figure 11 shows the experimental results of the MFRPLP-VEH under excitation accelerations of 8 m/s^2 and 12 m/s^2. It is observed that the theoretical model could effectively predict the experimental working frequency range of the MFRPLP-VEH. However, as the equivalent mass of Beam B being smaller than the others, when it is used as the drive beam, 20% error can be observed, especially in the output of beams A and C.

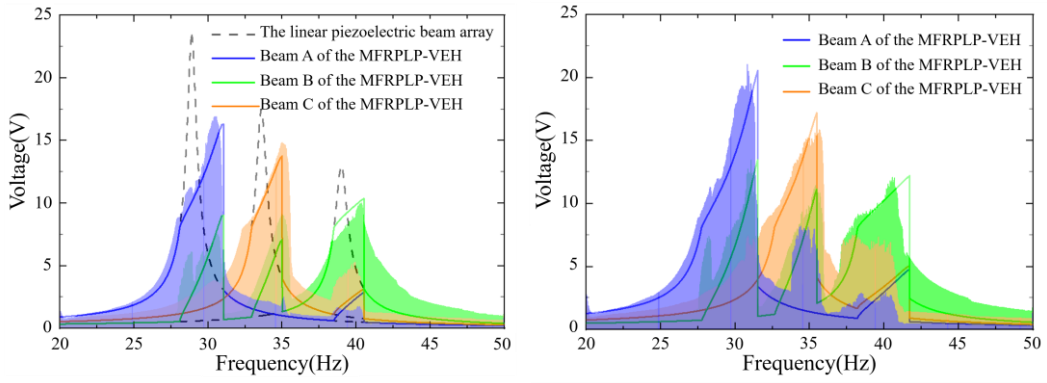

Figure 11 Comparison of the numerical and experimental results. (a) 8 m/s^2 and (b) 10 m/s^2.

The output voltage and output power can be used to evaluate the energy harvesting efficiency of the MFRPLP-VEH. A constant 25 μW source supply is usually used for low-powered wireless sensors (Zigbee, Bluetooth, etc). Therefore, a 5 V peak voltage is set as the threshold value for the effective working voltage while considering the energy loss and diode voltage drop. In this study, we use an output power of 25 μW to restrict the frequency range of the harvester, which is calculated based on the experimental data of the collision and non-collision vibrations with a constant acceleration of 10 m/s^2, as shown in Figure 12.

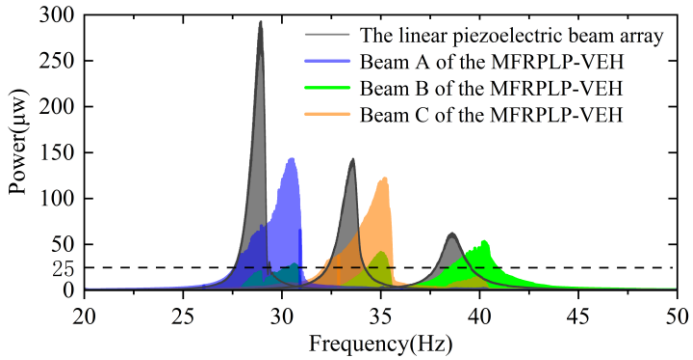

Figure 12 Comparison of the output power achieved in collision and no-collision modes (at a constant acceleration of 10 m/s^2).

Simulations are conducted using the proposed numerical model under the same excitation conditions. The effective working frequency range of beams A, B, and C are expanded from 29.2–30.7 Hz to 29.2–32.4 Hz, 33.7–35.2 Hz to 38.3–40.4 Hz, and 38.3–39.6 Hz to 33.7–36.1 Hz, respectively. Furthermore, the effective working frequency range of beams A, B, and C is expanded from 27.57–29.35 Hz to 26.64–30.96 Hz, 37.76–39.56 Hz to 38.31–40.91 Hz, and 32.26–34.2 Hz to 32.17–35.54 Hz, respectively. Table 2 shows a comparison of the bandwidth broadening effect of beams A, B, and C.

Table 2 Comparative analysis of the numerical and experimental results of the bandwidth broadening effect of the MFRPLP-VEH.

	Beam A	Beam B	Beam C	Total
Simulations broadening bandwidth (Hz)	1.5→3.2	1.5→2.4	1.3→2.1	4.3→7.1
Experiment broadening bandwidth (Hz)	1.78→3.32	1.94→3.37	1.8→2.6	5.52→9.26

As seen in Table 2, the total working frequency range of the MFRPLP-VEH is calculated as 67.8% in the experiment, indicating that the MFRPLP-VEH exhibits an improved broadband effect compared to the linear model. Moreover, the open-circuit voltages of beams A, B, and C measured at the resonant frequency clearly showed high-frequency components, as depicted in Figure 13. These high-frequency vibrations can be potentially harvested, with some of them having large variation levels.

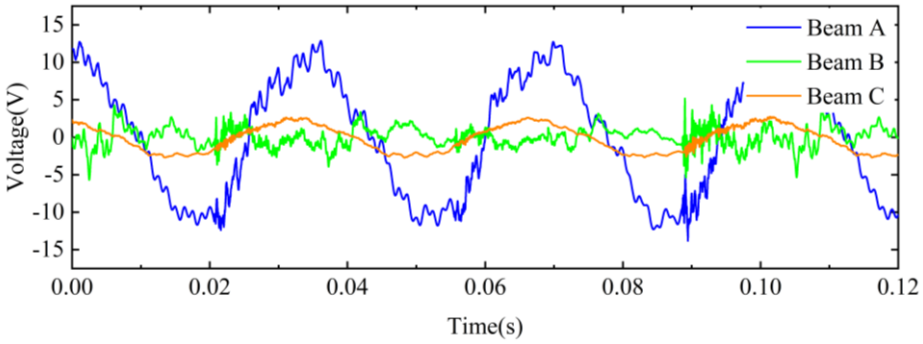

Figure 13 Open-circuit voltage of beams A, B, and C at the resonant frequency of Beam A.

4.2 Comparison of the capacitance charging

To further analyze the energy harvester efficiency of the MFRPLP-VEH, we conduct capacitive charging experiments for the MFRPLP-VEH and the linear model using frequency-swept excitation. The excitation conditions are kept the same as before. The piezoelectric beam is first connected to the interface circuit for rectification. Then, the three rectified circuits of the piezoelectric beams are connected in parallel to both ends of the capacitor. Figure 14 shows the circuit connection.

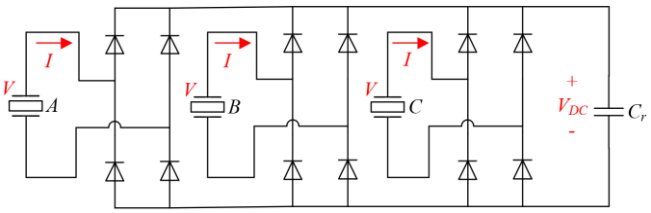

Figure 14 The capacitor charging circuit connection.

The linear piezoelectric beam array on the same plane and the MFRPLP-VEH are excited under the same excitation conditions (frequency sweeping from 20 Hz to 50 Hz, a constant acceleration amplitude of 10 m/s^2, a sweeping time of 200 s) and connected to the same circuit (The energy output of both is the sum of the three beams). The electric field energy stored in the two capacitors (Cr = 470 μF) is collected and calculated, as shown in Figure 15. In the initial phase of the frequency-swept excitation, the energy collected by the MFRPLP-VEH is roughly the same as that collected by the linear piezoelectric beam array. However, when the piezoelectric beams collide with each other, the MFRPLP-VEH collects much more electricity compared to the linear piezoelectric beam array. During the charging process of 200 s, the harvested energy of the MFRPLP-VEH and the linear piezoelectric beam array are calculated as 1.39 mJ and 0.71 mJ, respectively. Owing to the impact of high-frequency components and widening of the working frequency band, a multi-frequency response piecewise linear cantilever beam can potentially increase the generating capacity by 194% under the same excitation conditions.

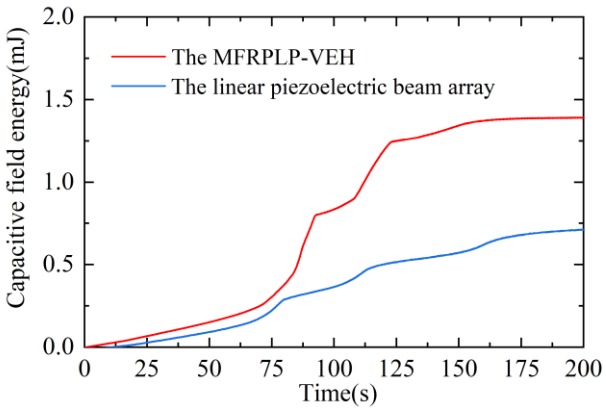

Figure 15 Comparison of the MFRPLP-VEH and the linear piezoelectric beam array in capacitance charging.

5. Conclusion

This study proposed a piecewise linear vibration energy harvester with a multi-frequency response to solve the issue of narrow working bandwidth and low efficiency in traditional

piezoelectric vibrational energy harvesters. The theoretical model for the proposed harvester was established based on factors such as electromechanical coupling and dynamic analysis, and its accuracy was verified experimentally. The proposed harvester has three resonance intervals, and each achieves a broadband effect through collision. As a result, the output power density and working frequency range are significantly enhanced. In detail, the energy generated by the MFRPLP-VEH is 194% of the energy generated by its linear counterpart under the same excitation conditions. However, future studies will concentrate on the optimization design of the harvester in a wider bandwidth and nonlinear collision modeling. We believe that the results of this study can provide meaningful guidance for designing broadband vibration energy harvesters.

Credit author statement

Bin Zhang: Conceptualization, Methodology, Validation. Haoyuan Li: Investigation, Data curation. Jinhui Liang: Writing - Original Draft, Data Curation, Investigation. Shengxi Zhou: Supervision, Visualization, Validation. Jun Gao: Supervision. Daniil Yurchenko: Writing-Reviewing and Editing, Visualization.

Conflicts of Interest

The author(s) declared no potential conflicts of interest with respect to the research, authorship, and/or publication of this article.

Acknowledgments

This project is supported by the National Natural Science Foundation of China (Grant nos. 51805298, 12072267, 12111530105), the Natural Science Foundation of Shandong Province (Grant no. ZR2019PEE015), the Young Scholars Program of Shandong University, Weihai (Grant no. 20820201004), the Fundamental Research Funds for the Central Universities (Grant no. 2019ZRJC006), and the Royal Society International Exchange 2020 Cost Share (NSFC) program with China IEC\NSFC\201127.

References

[1] Miao G, Fang S, Wang S, Zhou S. A low-frequency rotational electromagnetic energy harvester using a magnetic plucking mechanism. Applied Energy, 2022, 305: 117838. https://doi.org/10.1016/j.apenergy.2021.117838

[2] McKay I S, Wang E N. Thermal pulse energy harvesting. Energy, 2013, 57: 632-640. https://doi.org/10.1016/j.energy.2013.05.045

[3] Tan Y K, Panda S K. Energy harvesting from hybrid indoor ambient light and thermal energy sources for enhanced performance of wireless sensor nodes. IEEE Transactions on Industrial Electronics, 2010, 58(9): 4424-4435. https://ieeexplore.ieee.org/document/5675682/

[4] Yang K, Wang J, Yurchenko D. A double-beam piezo-magneto-elastic wind energy harvester for improving the galloping-based energy harvesting. Applied Physics Letters, 2019, 115(19): 193901. https://doi.org/10.1063/1.5126476

[5] Litak G, Friswell M I, Adhikari S. Magnetopiezoelastic energy harvesting driven by random excitations. Applied Physics Letters, 2010, 96(21): 214103. https://doi.org/10.1063/1.3436553

[6] Al Shami E, Wang Z, Wang X. Non-linear dynamic simulations of two-body wave energy converters via identification of viscous drag coefficients of different shapes of the submerged body based on numerical wave tank CFD simulation. Renewable Energy, 2021. https://doi.org/10.1016/j.renene.2021.07.068

[7] Zhang L, Zhang F, Qin Z, et al. Piezoelectric energy harvester for rolling bearings with capability of self-powered condition monitoring. Energy, 2021: 121770. https://doi.org/10.1016/j.energy.2021.121770

[8] Song R, Shan X, Lv F, et al. A novel piezoelectric energy harvester using the macro fiber composite cantilever with a bicylinder in water. Applied Sciences, 2015, 5(4): 1942-1954. https://doi.org/10.3390/app5041942

[9] Pathak S, Zhang R, Bun K, et al. Development of a novel wind to electrical energy converter of passive ferrofluid levitation through its parameter modelling and optimization. Sustainable Energy Technologies and Assessments, 2021, 48: 101641. https://doi.org/10.1016/j.seta.2021.101641

[10] Hwang W, Kim K B, Cho J Y, et al. Watts-level road-compatible piezoelectric energy harvester for a self-powered temperature monitoring system on an actual roadway. Applied Energy, 2019, 243: 313-320. https://doi.org/10.1016/j.apenergy.2019.03.122

[11] Zhang B, Li D Z, Li Y R, Ducharne B, Gao J. Double Peak Derived from Piezoelectric Coefficient Nonlinearity and Proposal for Self-Powered Systems. Transactions of Nanjing University of Aeronautics and Astronautics, 2018, 35(01):109-115. https://doi.org/10.16356/j.1005-

1120.2018.01.109

[12] Shen H, Qiu J, Balsi M. Vibration damping as a result of piezoelectric energy harvesting. Sensors and Actuators A: Physical, 2011, 169(1): 178-186. https://doi.org/10.1016/j.sna.2011.04.043

[13] Zhang H, Yuan W, Hao Y, et al. Influences of the feedthrough capacitance on the frequency synchronization of the weakly coupled resonators. IEEE Sensors Journal, 2015, 15(11): 6081-6088. https://doi.org/10.1109/JSEN.2015.2453401

[14] Gao M, Wang P, Jiang L, et al. Power generation for wearable systems. Energy & Environmental Science, 2021, 14(4): 2114-2157. https://doi.org/10.1039/D0EE03911J

[15] Liu W, Badel A, Formosa F, et al. A wideband integrated piezoelectric bistable generator: experimental performance evaluation and potential for real environmental vibrations. Journal of Intelligent Material Systems and Structures, 2015, 26(7): 872-877. https://doi.org/10.1177/1045389X14546660

[16] Bao B, Wang Q. A rain energy harvester using a self-release tank. Mechanical Systems and Signal Processing, 2021, 147: 107099. https://doi.org/10.1016/j.ymssp.2020.107099

[17] Bao B, Chen W, Wang Q. A piezoelectric hydro-energy harvester featuring a special container structure. Energy, 2019, 189: 116261. https://doi.org/10.1016/j.energy.2019.116261

[18] Liu Z, Wang X, Al Shami E, et al. A study of a speed amplified linear generator for low-frequency wave energy conversion. Mechanical Systems and Signal Processing, 2021, 149: 107226. https://doi.org/10.1016/j.ymssp.2020.107226

[19] Wu Y, Li S, Fan K, et al. Investigation of an ultra-low frequency piezoelectric energy harvester with high frequency up-conversion factor caused by internal resonance mechanism. Mechanical Systems and Signal Processing, 2022, 162: 108038. https://doi.org/10.1016/j.ymssp.2021.108038

[20] Gu Y, Liu W, Zhao C, et al. A goblet-like non-linear electromagnetic generator for planar multi-directional vibration energy harvesting. Applied Energy, 2020, 266: 114846. https://doi.org/10.1016/j.apenergy.2020.114846

[21] Fan K, Qu H, Wu Y, et al. Design and development of a rotational energy harvester for ultralow frequency vibrations and irregular human motions. Renewable Energy, 2020, 156: 1028-1039. https://doi.org/10.1016/j.renene.2020.04.117

[22] Jia Y. Review of nonlinear vibration energy harvesting: Duffing, bistability, parametric, stochastic and others. Journal of Intelligent Material Systems and Structures, 2020, 31(7): 921-944. https://doi.org/10.1177/1045389X20905989

[23] Ghayesh M H, Farokhi H. Nonlinear broadband performance of energy harvesters. International Journal of Engineering Science, 2020, 147: 103202. https://doi.org/10.1016/j.ijengsci.2019.103202

[24] Mallick D, Amann A, Roy S. Analysis of nonlinear spring arm for improved performance of vibrational energy harvesting devices. Journal of Physics: Conference Series. IOP Publishing, 2013, 476(1): 012088. https://doi.org/10.1088/1742-6596/476/1/012088

[25] Li H, Qin W, Lan C, et al. Dynamics and coherence resonance of tri-stable energy harvesting system. Smart Materials and Structures, 2015, 25(1): 015001. https://doi.org/10.1088/0964-1726/25/1/015001

[26] Deng W, Wang Y. Non-contact magnetically coupled rectilinear-rotary oscillations to exploit low-frequency broadband energy harvesting with frequency up-conversion. Applied Physics Letters, 2016, 109(13): 133903. https://doi.org/10.1063/1.4963786

[27] Meruane V, Pichara K. A broadband vibration-based energy harvester using an array of piezoelectric beams connected by springs. Shock and Vibration, 2016, 2016. https://doi.org/10.1155/2016/9614842

[28] Dechant E, Fedulov F, Fetisov L Y, et al. Bandwidth widening of piezoelectric cantilever Beam Arrays by mass-tip tuning for low-frequency vibration energy harvesting. Applied Sciences, 2017, 7(12): 1324. https://doi.org/10.3390/app7121324

[29] Ferrari M, Ferrari V, Guizzetti M, et al. Piezoelectric multifrequency energy converter for power harvesting in autonomous microsystems. Sensors and Actuators A: Physical, 2008, 142(1): 329-335. https://doi.org/10.1016/j.sna.2007.07.004

[30] Dhote S, Li H, Yang Z. Multi-frequency responses of compliant orthoplanar spring designs for widening the bandwidth of piezoelectric energy harvesters. International Journal of Mechanical Sciences, 2019, 157: 684-691. https://doi.org/10.1016/j.ijmecsci.2019.04.029

[31] Machado L Q, Yurchenko D, Wang J, et al. Multi-dimensional constrained energy optimization of a piezoelectric harvester for E-gadgets. iScience, 2021, 24(7): 102749.

https://doi.org/10.1016/j.isci.2021.102749

[32] Wei C, Jing X. Vibrational energy harvesting by exploring structural benefits and nonlinear characteristics. Communications in Nonlinear Science and Numerical Simulation, 2017, 48: 288-306. https://doi.org/10.1016/j.cnsns.2016.12.026

[33] Cao D X, Leadenham S, Erturk A. Internal resonance for nonlinear vibration energy harvesting. The European Physical Journal Special Topics, 2015, 224(14): 2867-2880. https://doi.org/10.1140/epjst/e2015-02594-4

[34] Zhao L C, Zou H X, Wu Z Y, et al. Dynamically synergistic regulation mechanism for rotation energy harvesting. Mechanical Systems and Signal Processing, 2021: 108637. https://doi.org/10.1016/j.ymssp.2021.108637

[35] Ma X, Li H, Zhou S, et al. Characterizing nonlinear characteristics of asymmetric tristable energy harvesters. Mechanical Systems and Signal Processing, 2022, 168: 108612. https://doi.org/10.1016/j.ymssp.2021.108612

[36] Wei C, Jing X. A comprehensive review on vibration energy harvesting: Modelling and realization. Renewable and Sustainable Energy Reviews, 2017, 74: 1-18. https://doi.org/10.1016/j.rser.2017.01.073

[37] Li M, Jing X. Novel tunable broadband piezoelectric harvesters for ultralow-frequency bridge vibration energy harvesting. Applied Energy, 2019, 255: 113829. https://doi.org/10.1016/j.apenergy.2019.113829

[38] Chen L Q, Jiang W A. Internal resonance energy harvesting. Journal of Applied Mechanics, 2015, 82(3). https://doi.org/10.1115/1.4029606

[39] Lu Z Q, Shao D, Fang Z W, et al. Integrated vibration isolation and energy harvesting via a bistable piezo-composite plate. Journal of Vibration and Control, 2020, 26(9-10): 779-789. https://doi.org/10.1177/1077546319889815

[40] Huang D, Chen J, Zhou S, et al. Response regimes of nonlinear energy harvesters with a resistor-inductor resonant circuit by complexification-averaging method. Science China Technological Sciences, 2021, 64(6): 1212-1227. https://doi.org/10.1007/s11431-020-1780-x

[41] Lu Z Q, Zhao L, Ding H, et al. A dual-functional metamaterial for integrated vibration isolation and energy harvesting. Journal of Sound and Vibration, 2021: 116251.

https://doi.org/10.1016/j.jsv.2021.116251

[42] Zhou S, Zuo L. Nonlinear dynamic analysis of asymmetric tristable energy harvesters for enhanced energy harvesting. Communications in Nonlinear Science and Numerical Simulation, 2018, 61: 271-284. https://doi.org/10.1016/j.cnsns.2018.02.017

[43] Li Z, Liu Y, Yin P, et al. Constituting abrupt magnetic flux density change for power density improvement in electromagnetic energy harvesting. International Journal of Mechanical Sciences, 2021, 198: 106363. https://doi.org/10.1016/j.ijmecsci.2021.106363

[44] Zhou S, Cao J, Inman D J, et al. Impact-induced high-energy orbits of nonlinear energy harvesters. Applied Physics Letters, 2015, 106(9): 093901. https://doi.org/10.1063/1.4913606

[45] Dai H, Wang Y K, Wang L. Nonlinear dynamics of cantilevered microbeams based on modified couple stress theory. International Journal of Engineering Science, 2015, 94: 103-112. https://doi.org/10.1016/j.ijengsci.2015.05.007

[46] Su M, Xu W, Zhang Y, et al. Response of a vibro-impact energy harvesting system with bilateral rigid stoppers under Gaussian white noise. Applied Mathematical Modelling, 2021, 89: 991-1003. https://doi.org/10.1016/j.apm.2020.07.022

[47] Pan P, Qin W Y, Yang Y F, et al. A collision impact based energy harvester using piezoelectric polyline beams with electret coupling. Journal of Physics D: Applied Physics, 2021, 54: 225502 https://doi.org/10.1088/1361-6463/abe968

[48] Zhao D, Wang X, Cheng Y, et al. Analysis of single-degree-of-freedom piezoelectric energy harvester with stopper by incremental harmonic balance method. Materials Research Express, 2018, 5(5): 055502. https://doi.org/10.1088/2053-1591/aabefc

[49] Fang S, Wang S, Miao G, et al. Comprehensive theoretical and experimental investigation of the rotational impact energy harvester with the centrifugal softening effect. Nonlinear Dynamics, 2020, 101(1): 123-152. https://doi.org/10.1007/s11071-020-05732-1

[50] Peng Y, Xu Z, Wang M, et al. Investigation of frequency-up conversion effect on the performance improvement of stack-based piezoelectric generators. Renewable Energy, 2021, 172: 551-563. https://doi.org/10.1016/j.renene.2021.03.064

[51] Soliman M S M, Abdel-Rahman E M, El-Saadany E F, et al. A wideband vibration-based energy harvester. Journal of Micromechanics and Microengineering, 2008, 18(11): 115021.

https://doi.org/10.1088/0960-1317/18/11/115021

[52] Lo C C. A cantilever Beam Chattering against a stop. Journal of Sound and Vibration, 1980, 69(2): 245-255. https://doi.org/10.1016/0022-460X(80)90609-4

[53] Tsai H C, Wu M K. Methods to compute dynamic response of a cantilever with a stop to limit motion. Computers & Structures, 1996, 58(5): 859-867. https://doi.org/10.1016/0045-7949(95)00174-F

[54] Liu H, Lee C, Kobayashi T, et al. Investigation of a MEMS piezoelectric energy harvester system with a frequency-widened-bandwidth mechanism introduced by mechanical stoppers. Smart Materials and Structures, 2012, 21(3): 035005. https://doi.org/10.1088/0964-1726/21/3/035005

[55] Le C P, Halvorsen E, et al. Wideband excitation of an electrostatic vibration energy harvester with power-extracting end-stops. Smart Materials and Structures, 2013, 22(7): 075020. https://doi.org/10.1088/0964-1726/22/7/075020

[56] Fang S, Wang S, Zhou S, et al. Exploiting the advantages of the centrifugal softening effect in rotational impact energy harvesting. Applied Physics Letters, 2020, 116(6): 063903. https://doi.org/10.1063/1.5140060

Modeling and analysis of a three-degree-of-freedom piezoelectric vibration energy harvester for broadening bandwidth

Bin Zhang[a,*], Haoyuan Li[a], Shengxi Zhou[b,*], Jinhui Liang[a], Jun Gao[a], Daniil Yurchenko[c]

[a] School of mechanical, Electrical & Information Engineering, Shandong University, Weihai, 264209, China.

[b] School of Aeronautics, Northwestern Polytechnical University, Xi'an 710072, China.

[c] Institute of Sound and Vibration Research, University of Southampton, Southampton, SO17 1BJ, UK.

*****Corresponding Author: zhoushengxi@nwpu.edu.cn (S. Zhou); bin.zhang@sdu.edu.cn (B. Zhang)

Abstract

This study proposes a multi-frequency response piecewise-linear piezoelectric vibration energy harvester (MFRPLP-VEH) by combining the linear multi-frequency resonance and nonlinear vibration bandwidth broadening methods to improve the working frequency bandwidth and environmental robustness of the piezoelectric vibration energy harvester. A theoretical model is established based on the electromechanical coupling and the dynamic response of the MFRPLP-VEH. The energy harvesting performance and broadening width efficiency of the MFRPLP-VEH were obtained through an experimental verification platform. An error rate of 5% is observed between the numerical results of the theoretical model and the experiment results. Furthermore, the operating frequency range is widened by 67.8% at an external excitation acceleration of 10 m/s^2. The energy generated by the MFRPLP-VEH is 194% of the energy generated by its linear counterpart under the same excitation conditions. The numerical and experimental results verify the accuracy of the theoretical model and the broadband working frequency range of the MFRPLP-VEH.

Keywords: Piezoelectric energy harvesting; Electromechanical coupling; Broadband; Nonlinear; Multi-frequency

1. Introduction

Given the increasing applications of low-power consumption sensor networks, reliable energy supply technologies have become a research focus. Chemical batteries, however, have

limited service life, high replacement, and maintenance costs, and are not environmentally friendly. Therefore, there is an urgent need for developing new energy sources that exhibit long service life, compact size, are light weight, and environmental friendly to compensate for the shortcomings of traditional chemical batteries. An alternative energy solution is by converting energy sources such as kinetic energy, thermal energy, light energy, and wind energy collected from the ambient environment into electric energy [1-4]. Therefore, different energy harvesters were designed and tested [5-9]. For example, a piezoelectric vibration energy harvester can power low-energy consumption devices and sensors by converting vibration energy into electricity [10–15]. However, because the natural vibration excitations have relatively low frequency and intensity, the harvester is usually designed to magnify the amplitude [16, 17], speed [18], and frequency [19–21]. Furthermore, the output power is highly dependent on the resonance of the harvester exhibiting external excitation, which is not always constant [22]. Therefore, researchers have proposed multiple designs of energy harvesters to broaden the working frequency range of the piezoelectric vibration energy harvester through theories and experiments [23–25]. The existing methods used to broaden the frequency range of the harvester can be divided into two categories:

One is the linear multi-frequency resonance method, wherein a harvester is designed to have multiple resonant frequencies within the frequency range of the vibration source and generates multiple resonant peaks [26–28]. Ferrari *et al.* [29] proposed a piezoelectric vibrational energy harvester with three cantilever beams arranged in an array structure. The cantilever beams exhibit their own resonant frequency due to their different structures. Once the external vibration source is close to either of the three resonant frequencies, the corresponding Beam Can significantly increase the output power. Dhote *et al.* [30] designed a harvester using multiple multi-mode cantilever beams in the same plane. The cantilever beams exhibited multi-mode characteristics and generated multi-step resonant frequencies to achieve a broadband frequency range. Results showed that due to the linear multi-frequency resonance, the different vibration units effectively expanded the working frequency range by accumulating the working frequency band. Recently, a global device optimization procedure was proposed for an energy harvester comprising an array of beams. While the proposed design was used to increase the

power density and not the bandwidth, it proved to be effective and resulted in a remarkable 0.3 W power output for the gravity-based device [31]. However, the working frequency band was limited around the resonant frequency because the harvester was still linear. Moreover, the working frequency range of a single vibration unit remained unchanged, which increased the volume of the harvester and decreased the output power density.

The second method is the nonlinear frequency-broadening method. Compared with linear harvester, elaborately introduced nonlinearity, such as structural design [32, 33], magnetic force [34, 35] and other methods [36], could increase the operation bandwidth of the energy harvester, which is conducive to energy harvesting. Li *et al*. [37] investigated a nonlinear X-shaped piezoelectric energy harvester with horizontal and vertical installation configurations, which can achieve tunable bandwidth harvesting by adjusting its structural parameters. Internal resonance is explored to enhance vibration-based energy harvesting by Chen *et al* [38]. Under the influence of internal resonances, the amplitude-frequency response curves have two peaks bending to the left and right respectively. As the results, the internal resonance design produces more power than other designs especially under the Gaussian white noise and the exponentially correlated noise. Lu *et al*. [39] designed a bistable piezo-composite plate for both vibration isolation and energy harvesting, predicted analytically the hardening nonlinearity bending of the amplitude–frequency response curves. The results show that the bistable piezo-composite plate improves the feasibility and effectiveness of the integrated design. Magnetic forces have also been used to broaden the frequency to enhance energy harvesting devices [40 – 43]. Zhou *et al.* [44] presented an impact-induced method for nonlinear energy harvesters to obtain high-energy orbits over a wide frequency range under low excitation levels. Results showed that the working bandwidth significantly enhanced the energy-harvesting performance under low excitation levels. Dai *et al*. [45] studied nonlinear modeling and dynamic analysis of cantilever microbeams and explored the effect of the size of material microstructures on the energy harvesting performance. The frequency response curve exhibited clear softening-type behavior under harmonic excitations. In addition, collisional piecewise nonlinearity is also an effective means to improve the performance of the harvester [46, 47]. A piecewise linear design was used to broaden the working frequency range of the energy harvester through collisions between the

vibration components and the limiter, which changes the equivalent stiffness of the harvester to attain the effect of nonlinear characteristics [48, 49]. Peng *et al.* [50] introduced the impact frequency-up conversion effect into stacked piezoelectric energy harvester structures. Compared to the control group without truncation, the average power is enhanced by over 177 times and the matched resistance is significantly reduced from over 5 kΩ to 73.10 Ω. Soliman *et al.* [51] proposed a piecewise-linear magnetic-electric vibration energy harvester by placing a stopper within the vibration range of the cantilever beam. When the amplitude of the piezoelectric cantilever beam is greater than the clearance, a collision occurs between the beam and the retaining block, which changes the equivalent stiffness of the beam in the piecewise linear mode. As a result, the overall performance of the energy harvester was nonlinear. Furthermore, results showed that the piecewise linear method could effectively broaden the operating frequency of the harvester. The above methods can successfully broaden the working frequency range of harvesters and improve the energy harvesting efficiency.

This study proposes the multi-frequency response piecewise-linear piezoelectric vibration energy harvester (MFRPLP-VEH) by combining the linear multi-frequency resonance method and the nonlinear frequency broadening method to further enhance the performance of the piezoelectric vibration energy harvester and its environmental robustness. The three cantilever beams of the MFRPLP-VEH are active and colliding beams, whose coupling effect exhibits nonlinear characteristics. Then a theoretical model is established based on the electromechanical coupling and the dynamic response of the MFRPLP-VEH. All the outputs of the collision beams are carefully considered and modeled. In order to validate the broadband performance and energy harvesting efficiency of the proposed MFRPLP-VEH, an experimental setup is developed. This design expands the working frequency band of the vibration energy harvester and makes it possible to have a continuous and stable output.

2. Modeling

As shown in Figure 1, the proposed MFRPLP-VEH comprises a base structure and three piezoelectric cantilever beams with adjacent resonant frequencies. Each piezoelectric beam is fabricated using piezoelectric patches and structural alloy steel for the substrate layer having the same dimension parameters. The tip masses are different owing to the different resonant

frequencies of the cantilever beams. Table 1 summarizes the dimensions and material parameters of the piezoelectric cantilever beams.

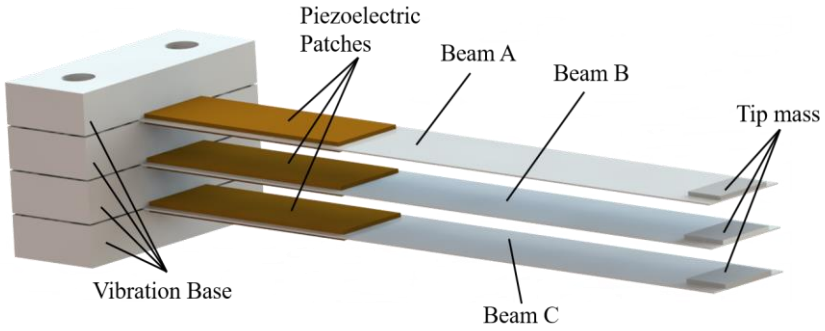

Figure 1 The proposed MFRPLP-VEH.

Table 1 Parameters of the cantilever piezoelectric beams.

Parameter	Value
Beam length	100 mm
Beam width	12 mm
Beam thickness	0.2 mm
Beam density	7900 kg/m^3
Young's modulus of the beam	120 Gpa
The tip mass of Beam A	0.5 gram
The tip mass of Beam B	0 gram
The tip mass of Beam C	0.3 gram
PZT length	30 mm
PZT width	10 mm
PZT thickness	0.4 mm
PZT density	7600 kg/m^3
Piezoelectric capacitance	26.5 nF
Piezoelectric constant	150×10^{-12} m/V
Permittivity of the PZT	1800
Young's modulus of the PZT	80 Gpa

The vibration exciter drives the cantilever beam to vibrate vertically to generate a bending moment, and the piezoelectric patches convert the mechanical vibration energy into electricity.

Once the relative displacement of the two piezoelectric beams is greater than the gap, the beams collide. During periodic motion, the collision causes the stiffness to be nonlinear. The three double-crystal piezoelectric beams are denoted as beams A, B, and C, from top to bottom, and have resonant frequencies of $f_A<f_C<f_B$, respectively. When the frequency sweeps from low to high, Beam A resonates first. When the amplitude of vibration exceeds gap d_1 between beams A and B, they begin to collide. As the excitation frequencies increase, Beam A breaks out of resonance, and its amplitude gradually decreases with no collision. The amplitude of Beam C gradually increases, and it begins to resonate. When the amplitude of vibration exceeds gap d_2 between beams B and C, they begin to collide. As the excitation frequencies increase further, Beam C breaks out of resonance while Beam B continues to resonate and collide with the other two beams.

Giving that the dynamic behavior of mechanical collisions is very complex, the exact results of the vibration response are rarely obtained. Therefore, a variety of average or approximate methods have been developed to give the nonlinear solution [52, 53]. The MFRPLP-VEH is theoretically analyzed by combining the equivalent spring-mass-damping model with piecewise linear springs. Furthermore, to analyze the energy harvesting performance of each beam individually, the damping of the resonant beam is considered, whereas the damping of the non-resonant beams is disregarded [54]. Then, modeling analysis was performed for beams A, B, and C. Figure 2 shows the schematic model of the MFRPLP-VEH.

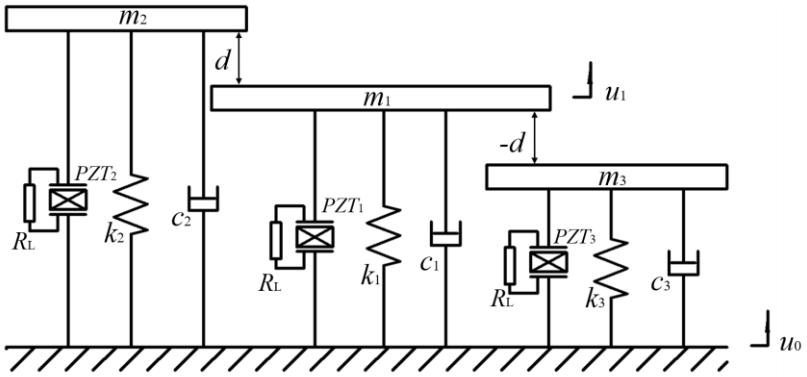

Figure 2 Schematic model of the MFRPLP-VEH.

As shown in Figure 2, subscripts 1, 2 and 3 refer to beams A, B, and C, respectively. We consider the collision of any two beams for analysis. m_1 is the equivalent vibration mass. k_1 is the equivalent stiffness, and c_1 is the equivalent damping of the resonant beam. m_2 (m_3), k_2 (k_3),

and c_2(c_3) are the equivalent mass, stiffness, and damping of the impact beams, respectively. PZTs ($_{1\text{-}2\text{-}3}$) are piezoceramics bonded to beams A, B, and C, respectively. $u_0(t)$ and $u_1(t)$ represent the external excitation and displacement of the resonant beam, respectively. The motion of the resonant beam can be classified into free vibration motion and collision motion. The stiffness and damping of the resonant beam remain unchanged when the relative displacement u_1-u_0 is smaller than the clearance d and change when the two cantilever beams collide. Note that the collision time is kept short for the convenience of the theoretical modeling and analysis [55, 56] and the pre-impact momentums of the beams are small. Furthermore, the speed of the two beams after the collision is assumed to be the same, and the collision beams obey the conservation law of momentum. In other words, the collision is completely inelastic. Based on these assumptions, the stiffness and damping of the two beams would be connected in parallel. The corresponding nonlinear motion equation is given as:

$$m(\ddot{y}+\ddot{y}_0)+c_1\dot{y}+k_1y+f(\dot{y},y)+F_p=0 \tag{1}$$

Herein, y_0=u_0(t)=Ucos(ωt), where U and ω represent the excitation amplitude and excitation frequency, respectively. $f(\dot{y},y)$ in Eq. (1) represents the nonlinear term of the MFRPLP-VEH and is given as:

$$f(\dot{y},y)=\begin{cases} c_1\dot{y}+k_1(y+d) & (y>d) \\ 0 & (y\le d) \end{cases}$$

Because the mechanical model ignores the electromechanical coupling, a significant error was observed between the theoretical derivation and experimental results. Therefore, piezoelectric damping caused by the external load could improve the model accuracy.

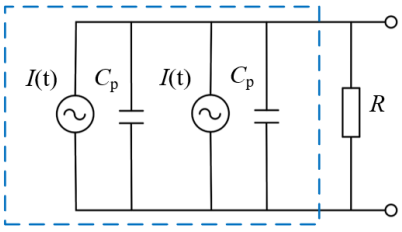

Figure 3 Equivalent circuit of a piezoelectric beam (with two piezoelectric patches connected in parallel).

$I_{up}(t)$ and $I_{down}(t)$ are the two piezoelectric patches pasted on both sides of the piezoelectric beam. Figure 3 shows the bimorph equivalent circuit. The total equivalent capacitance C_p and

current $I(t)$ (sum of I_{up} and I_{down}) of the bimorph piezoelectric cantilever beam are given as:

$$C_p = \frac{L_p W_p \varepsilon_p}{2T_p} \tag{2}$$

$$I(t) = -\Theta \dot{y} \tag{3}$$

According to Kirchhoff's law, the governing equation of the circuit is obtained as:

$$C_p \dot{v} + v / R = \Theta \dot{y} \tag{4}$$

where L_p, W_p, and T_p in Equation (2) represent the length, width, and thickness of the piezoelectric patch, respectively, and ε_p is the dielectric constant of the piezoelectric material. In Equation (4), Θ is the electromechanical coupling coefficient, and v is the open-circuit voltage at both ends of the piezoelectric patch.

Therefore, the nonlinear governing equations are given as:

$$\begin{cases} m(\ddot{y} + \ddot{y}_0) + c_1 \dot{y} + k_1 y + f(\dot{y}, y) + F_p = 0 \\ C_p \dot{v} + v / R = \Theta \dot{y} \end{cases} \tag{5}$$

3. Dynamic analysis

The nonlinear differential equation of the MFRPLP-VEH has been described in the previous section. Furthermore, the asymptotic method (average method) is adopted to solve the set of coupled equations of motion. To better understand the theoretical model, we derive the following equation from Equation (5):

$$\begin{cases} \ddot{y}_0 + \dfrac{c_1}{m}\dot{y} + \dfrac{\Theta V(t)}{m} + \dfrac{1}{m} f(\dot{y}, y) = -\ddot{y} - \dfrac{k_1}{m} y \\ \dot{V}(t) + \dfrac{1}{RC_p} V(t) - \dfrac{\Theta}{C_p} \dot{y} = 0 \end{cases} \tag{6}$$

The left side of the first equation is the external excitation term, where $\ddot{y}_0$, mechanical damping, $\frac{c_1}{m}\dot{y}$, piezoelectric damping term, and $f(\dot{y}, y)$ is the nonlinear term. In the occurrence of a nonlinear vibration collision, the terms on the left have less influence on the vibration response than the linear terms on the right, which can be temporarily ignored. Therefore, a new parameter B_p is introduced, which represents the sum of the four terms on the left, and ε is used as the prefix to indicate an infinitesimal quantity. Therefore, Equation (6) can be further simplified as:

$$\begin{cases} \varepsilon B_{\mathrm{p}} = -\ddot{y} - x_1 y \\ \dot{V}(t) - x_2 \dot{y} + x_3 V(t) = 0 \end{cases} \tag{7}$$

where the newly introduced parameters x_1, x_2, x_3 are given as:

$$x_1 = \frac{k_1}{m},\ x_2 = \frac{\Theta}{C_{\mathrm{p}}},\ x_3 = \frac{1}{RC_{\mathrm{p}}}, \tag{8}$$

and B_{p} is given as:

$$B_{\mathrm{p}} = \ddot{y}_0 + \frac{c_1}{m}\dot{y} + \frac{1}{m} f(\dot{y}, y) + \frac{\Theta}{m} V(t) \tag{9}$$

After introducing $\varepsilon B_{\mathrm{p}}$, Equation (6) can be further simplified to solve the collision energy harvesting motion, as

$$\begin{cases} \ddot{y} + x_1 y = 0 \\ \dot{V}(t) - x_2 \dot{y} + x_3 V(t) = 0 \end{cases} \tag{10}$$

By solving Equation (10), we obtain the solution of Equation (5) as:

$$\begin{cases} y = D\cos\theta \\ \dot{y} = -\omega_n D\sin\theta \\ V(t) = \left(\dfrac{\omega_n^2 x_2}{\omega_n^2 + x_3^2}\cos\theta - \dfrac{\omega_n x_2 x_3}{\omega_n^2 + x_3^2}\sin\theta \right) D \\ \theta = \omega t + \varphi \\ \omega_n = \sqrt{x_1} \end{cases} \tag{11}$$

where D is the amplitude of the system displacement y, θ is the phase angle of y, ω_n corresponds to the natural frequency of the linear system, and φ is the phase difference between θ and the phase angle of the external excitation. The nonlinear part of the MFRPLP-VEH can be solved by eliminating the infinitesimal quantity ε after the linear system solution is obtained.

The displacement amplitude D is given as:

$$D = \frac{A_0 \omega^2}{\sqrt{\left(\lambda^2(D) - \omega^2\right)^2 + 4\delta^2(D)\omega^2}} \tag{12}$$

The phase difference φ is given as:

$$\varphi = \tan^{-1}\left[-\frac{2\delta(D)\omega}{\lambda^2(D) - \omega^2} \right] \tag{13}$$

The coefficient $\delta(D)$ of the nonlinear amplitude function is given as:

$$\delta(D) = \frac{c_1}{2m} - \frac{\Theta x_2 x_3}{2m\left(\omega_n^2 + x_3^2\right)} - \frac{c_2}{2\pi m} G \tag{14}$$

The equivalent natural frequency $\lambda(D)$ of the MFRPLP-VEH is given as:

$$\lambda(D) = \omega_n + \frac{\Theta \omega_n x_2}{2m\left(\omega_n^2 + x_3^2\right)} - \frac{k_2}{2\pi\omega_n m} G \tag{15}$$

To plot the amplitude-frequency curve, ω is derived from Equation (12) as:

$$\omega = \sqrt{\frac{\left(\lambda^2 - 2\delta^2(D)\right) \pm \sqrt{\left(\lambda^2 - 2\delta^2(D)\right)^2 - \left(1-h^2\right)\lambda^4(D)}}{1-h^2}} \tag{16}$$

where $h = A_0 / D$ is the displacement amplitude ratio between the external excitation and the MFRPLP-VEH.

When continuous amplitude D is known, $\delta(D)$ and $\lambda(D)$ can be calculated by substituting Equations (14) and (15) in Equation (16) to obtain the corresponding value of ω. According to Equation (11), the relationship between the output voltage and displacement of the energy collection system can be deduced as:

$$\begin{aligned} V &= \frac{\omega_n x_2}{\sqrt{\omega_n^2 + x_3^2}} D \\ \theta_1 &= \theta + \varphi_1 \end{aligned} \tag{17}$$

where the phase difference ϕ_1 is given as:

$$\varphi_1 = \tan^{-1} \frac{x_3}{\omega_n} \tag{18}$$

To obtain the relationship between the output voltage V and external excitation frequency ω, we set $\gamma = \frac{\sqrt{\omega_n^2 + x_3^2}}{\omega_n x_2}$ and substitute Equation (17) into Equation (16) as:

$$\omega = \sqrt{\frac{\left(\omega_n^2 - 2\delta^2(D)\right) \pm \sqrt{\left(\omega_n^2 - 2\delta^2(D)\right)^2 - \left(1 - \left(\frac{A_0}{\gamma V}\right)^2\right)\lambda^4(D)}}{1 - \left(\frac{A_0}{\gamma V}\right)^2}} \tag{19}$$

The piezoelectric patches are considered as a current source containing internal resistance:

$$R_{\mathrm{p}} = \frac{1}{2\pi f C_{\mathrm{p}}} \tag{20}$$

Therefore, the output power of the MFRPLP-VEH can be obtained as:

$$P = \frac{V^2 R}{(R_p + R)^2} \tag{21}$$

Beam A is used as an example to explain the working principle of the collision. As shown in Figure 4, the simulation was carried out using Equation (19), and the parameters are listed in Table 1.

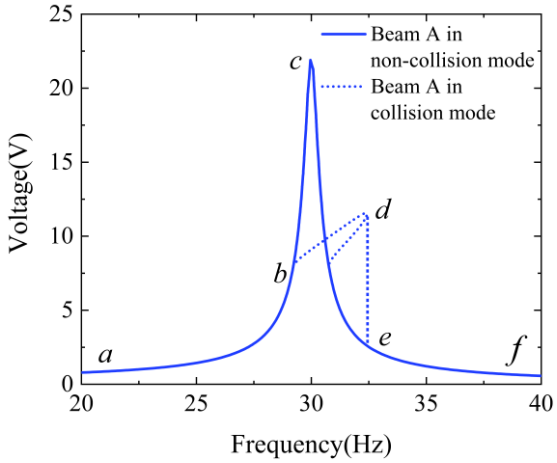

Figure 4 Voltage-frequency characteristic curve of Beam A (at excitation acceleration of 10 m/s^2).

The collision clearance between beams A and B was set to 5 mm. As the excitation frequency gradually increased, the output voltage of Beam A increased from point *a* to point *b*. When the excitation frequency reaches point *b*, the relative displacements of beams A and B become larger than the clearance *d*, and a collision occurs. As a result, the voltage amplitude-frequency curve of Beam A starts to deflate from point *b* to point *d* and is no longer the same as that of the original linear system (solid line). On reaching point *d*, the amplitude drops directly from point *d* to the corresponding amplitude of the linear system at point *e*. The amplitude continues to decline along the linear amplitude-frequency curve.

Similarly, we can obtain the voltage amplitude-frequency curve based on the simulations of the voltage amplitude-frequency curve when the three beams collide with each other in turns, as shown in Figure 5. For example, when Beam B starts to resonate at approximately 40 Hz, it collides with beams A and C considering the clearances are the same. Both the resonant and collision beams generate electricity. The effective working bandwidth can be broadened significantly to enhance the vibration energy under a large bandwidth variation.

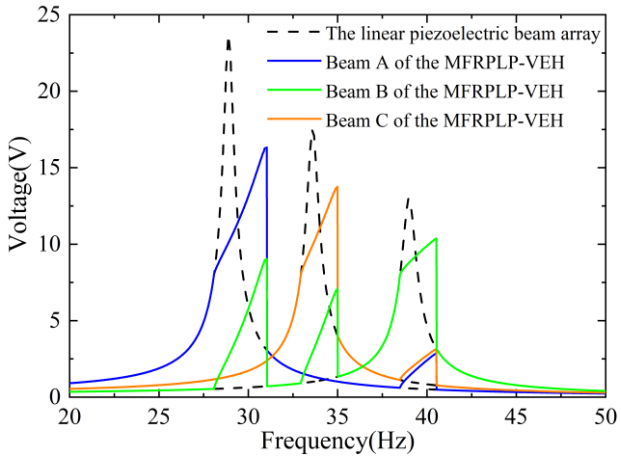

Figure 5 Numerical voltage amplitude-frequency curves of the MFRPLP-VEH and the linear piezoelectric beam array.

4. Experiments and discussion

To verify the three-dimensional model structure of the MFRPLP-VEH, three bimorph cantilever beams with adjacent resonant frequencies are fabricated, as shown in Figure 6. Two piezoelectric patches are bonded in a parallel connection in the opposite polarization directions. The parameters of the fabricated MFRPLP-VEH are listed in Table 1.

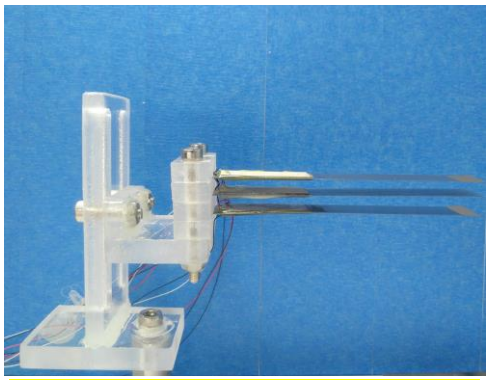

Figure 6 The MFRPLP-VEH in experiment.

Figure 7 shows the experimental setup, which is comprised an arbitrary function generator (Tektronix-AFG1062), power amplifier (YE5874A), shaker (JZK-50), digital oscilloscope (Rohde & Schwarz RTB2004), laser vibrometer (Keyence LK-GD500), and a noise current preamplifier (SR570-Low). A frequency-swept signal is generated by the function generator to control the power amplifier, which in turn is connected to the shaker. An accelerometer is used to monitor the output acceleration. The current and voltage of the MFRPLP-VEH are measured using a current amplifier and an oscilloscope.

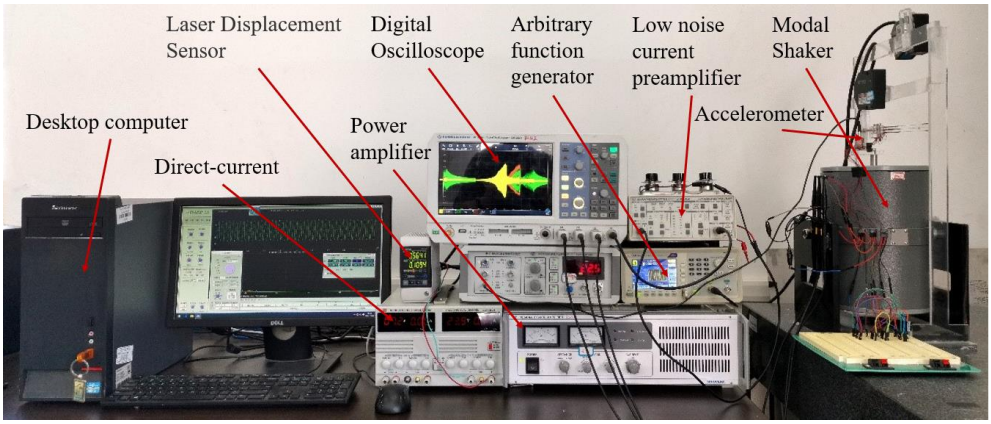

(a)

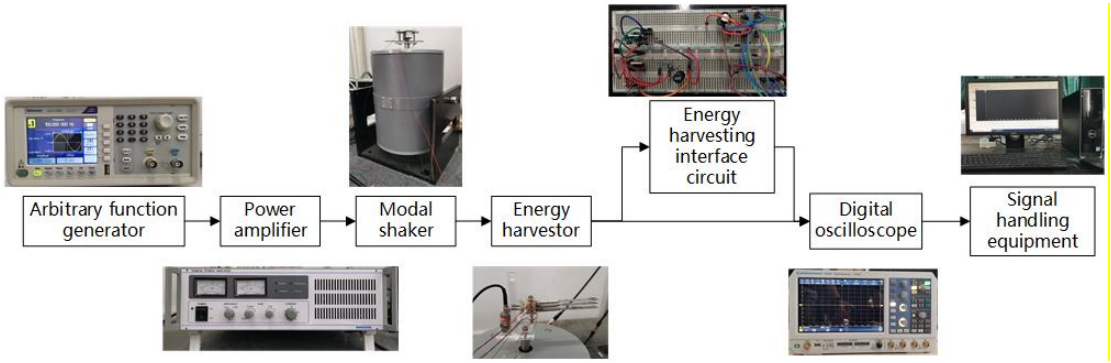

(b)

Figure 7 (a) Experimental setup; (b) flow diagram with experimental devices.

4.1 Output and bandwidth broadening experiment

First, the voltages of the piezoelectric beams are recorded by exciting the beams individually under a constant acceleration of 10 m/s^2 (frequency sweeping from 20 Hz to 50 Hz, sweeping time of 200 s), as shown in Figure 8. As the excitation acceleration remained unchanged, the peak value of the voltage decreased, and the frequency increased. The free vibration mode measurements are in good agreement with the simulations shown in Figure 5. The resonant frequencies of beams A, B, and C in experiment are calculated as 28.9, 33.6, and 38.6 Hz, respectively.

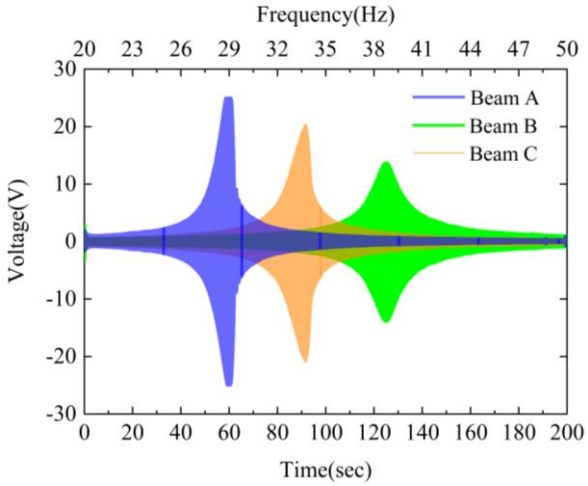

Figure 8 Individual tests (non-collision) of the frequency-swept voltage response curves of each beam under a constant acceleration of 10 m/s^2 (frequency sweeping from 20 Hz to 50 Hz, sweeping time of 200 s).

Impedance matching is performed for each piezoelectric beam at their corresponding resonant frequencies. The output voltage and output power curves, along with the external load impedance, can be obtained, as shown in Figure 9.

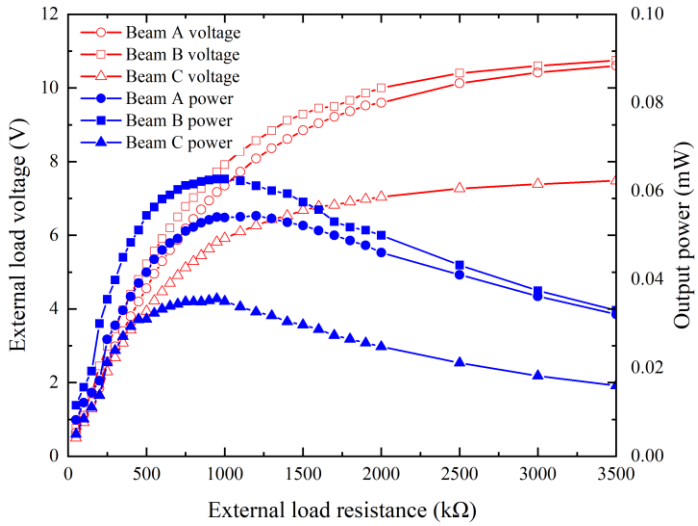

Figure 9 Non-collision output voltage and power curve versus the external load impedance of the MFRPLP-VEH.

As shown in Figure 9, as the external load impedance increases, the output voltage gradually increases until it converges with the open-circuit voltage of the harvester. Simultaneously, the maximum output power of each piezoelectric beam increases as the external load impedance increases. When the external load impedance reaches a peak value, the maximum output power decreases gradually. Then, we conducted the frequency-swept collision experiments at 8 m/s^2,

10 m/s^2, 12 m/s^2, and 14 m/s^2 with the same frequency-swept setting. The experimental results are shown in Figure 10.

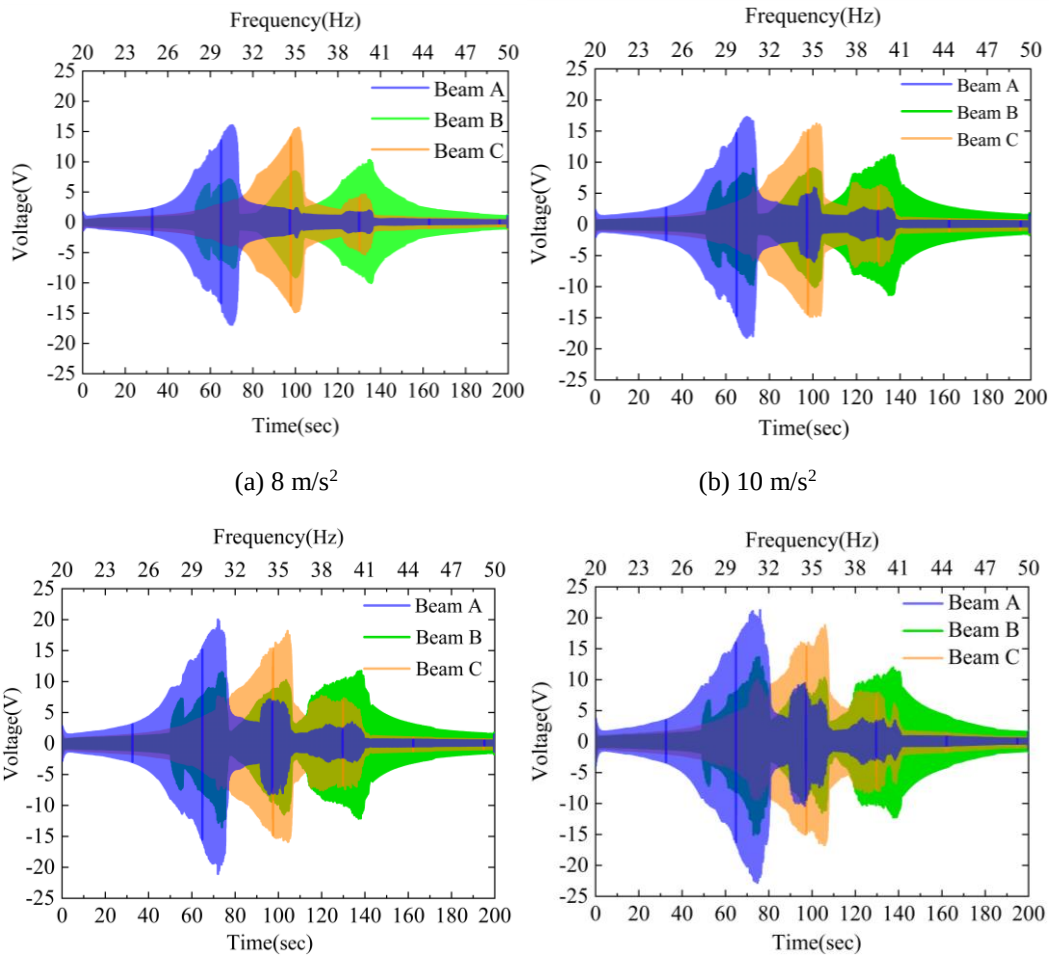

(a) 8 m/s^2 (b) 10 m/s^2

(c) 12 m/s^2 (d) 14 m/s^2

Figure 10 The frequency-swept voltage response curve of MFRPLP-VEH under different acceleration excitations (the frequency sweeping from 20 Hz to 50 Hz, the sweeping time of 200s).

The numerical and experimental results are compared to verify the theoretical model. Figure 11 shows the experimental results of the MFRPLP-VEH under excitation accelerations of 8 m/s^2 and 12 m/s^2. It is observed that the theoretical model could effectively predict the experimental working frequency range of the MFRPLP-VEH. However, as the equivalent mass of Beam B being smaller than the others, when it is used as the drive beam, 20% error can be observed, especially in the output of beams A and C.

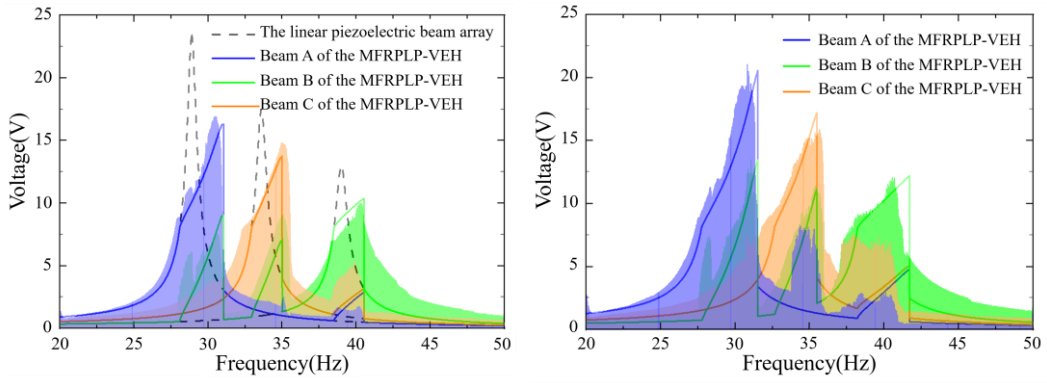

Figure 11 Comparison of the numerical and experimental results. (a) 8 m/s^2 and (b) 10 m/s^2.

The output voltage and output power can be used to evaluate the energy harvesting efficiency of the MFRPLP-VEH. A constant 25 μW source supply is usually used for low-powered wireless sensors (Zigbee, Bluetooth, etc). Therefore, a 5 V peak voltage is set as the threshold value for the effective working voltage while considering the energy loss and diode voltage drop. In this study, we use an output power of 25 μW to restrict the frequency range of the harvester, which is calculated based on the experimental data of the collision and non-collision vibrations with a constant acceleration of 10 m/s^2, as shown in Figure 12.

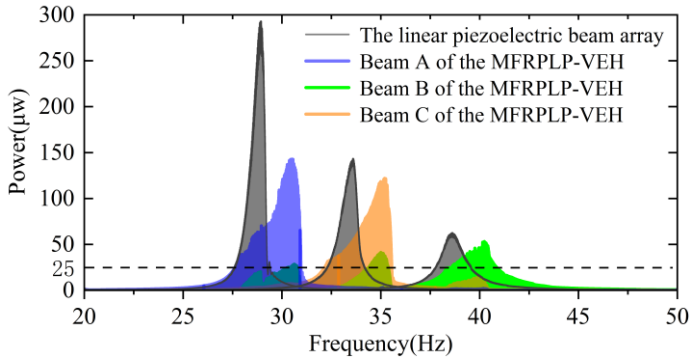

Figure 12 Comparison of the output power achieved in collision and no-collision modes (at a constant acceleration of 10 m/s^2).

Simulations are conducted using the proposed numerical model under the same excitation conditions. The effective working frequency range of beams A, B, and C are expanded from 29.2–30.7 Hz to 29.2–32.4 Hz, 33.7–35.2 Hz to 38.3–40.4 Hz, and 38.3–39.6 Hz to 33.7–36.1 Hz, respectively. Furthermore, the effective working frequency range of beams A, B, and C is expanded from 27.57–29.35 Hz to 26.64–30.96 Hz, 37.76–39.56 Hz to 38.31–40.91 Hz, and 32.26–34.2 Hz to 32.17–35.54 Hz, respectively. Table 2 shows a comparison of the bandwidth broadening effect of beams A, B, and C.

Table 2 Comparative analysis of the numerical and experimental results of the bandwidth broadening effect of the MFRPLP-VEH.

	Beam A	Beam B	Beam C	Total
Simulations broadening bandwidth (Hz)	1.5→3.2	1.5→2.4	1.3→2.1	4.3→7.1
Experiment broadening bandwidth (Hz)	1.78→3.32	1.94→3.37	1.8→2.6	5.52→9.26

As seen in Table 2, the total working frequency range of the MFRPLP-VEH is calculated as 67.8% in the experiment, indicating that the MFRPLP-VEH exhibits an improved broadband effect compared to the linear model. Moreover, the open-circuit voltages of beams A, B, and C measured at the resonant frequency clearly showed high-frequency components, as depicted in Figure 13. These high-frequency vibrations can be potentially harvested, with some of them having large variation levels.

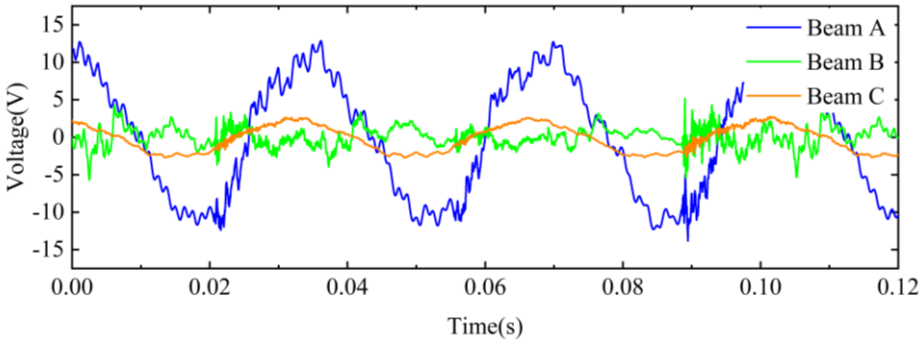

Figure 13 Open-circuit voltage of beams A, B, and C at the resonant frequency of Beam A.

4.2 Comparison of the capacitance charging

To further analyze the energy harvester efficiency of the MFRPLP-VEH, we conduct capacitive charging experiments for the MFRPLP-VEH and the linear model using frequency-swept excitation. The excitation conditions are kept the same as before. The piezoelectric beam is first connected to the interface circuit for rectification. Then, the three rectified circuits of the piezoelectric beams are connected in parallel to both ends of the capacitor. Figure 14 shows the circuit connection.

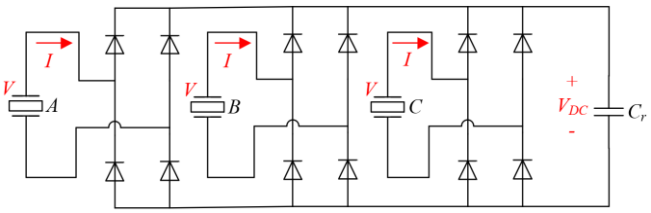

Figure 14 The capacitor charging circuit connection.

The linear piezoelectric beam array on the same plane and the MFRPLP-VEH are excited under the same excitation conditions (frequency sweeping from 20 Hz to 50 Hz, a constant acceleration amplitude of 10 m/s^2, a sweeping time of 200 s) and connected to the same circuit (The energy output of both is the sum of the three beams). The electric field energy stored in the two capacitors (Cr = 470 μF) is collected and calculated, as shown in Figure 15. In the initial phase of the frequency-swept excitation, the energy collected by the MFRPLP-VEH is roughly the same as that collected by the linear piezoelectric beam array. However, when the piezoelectric beams collide with each other, the MFRPLP-VEH collects much more electricity compared to the linear piezoelectric beam array. During the charging process of 200 s, the harvested energy of the MFRPLP-VEH and the linear piezoelectric beam array are calculated as 1.39 mJ and 0.71 mJ, respectively. Owing to the impact of high-frequency components and widening of the working frequency band, a multi-frequency response piecewise linear cantilever beam can potentially increase the generating capacity by 194% under the same excitation conditions.

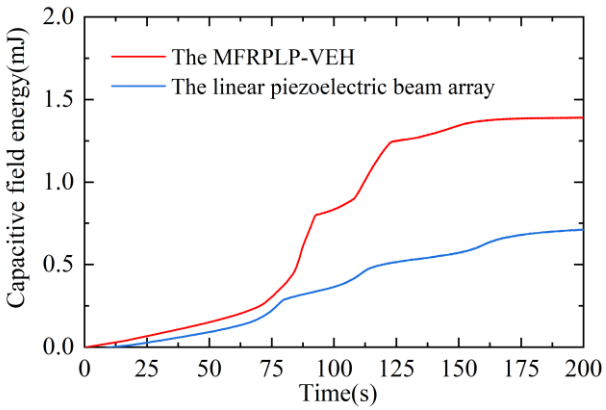

Figure 15 Comparison of the MFRPLP-VEH and the linear piezoelectric beam array in capacitance charging.

5. Conclusion

This study proposed a piecewise linear vibration energy harvester with a multi-frequency response to solve the issue of narrow working bandwidth and low efficiency in traditional

piezoelectric vibrational energy harvesters. The theoretical model for the proposed harvester was established based on factors such as electromechanical coupling and dynamic analysis, and its accuracy was verified experimentally. The proposed harvester has three resonance intervals, and each achieves a broadband effect through collision. As a result, the output power density and working frequency range are significantly enhanced. In detail, the energy generated by the MFRPLP-VEH is 194% of the energy generated by its linear counterpart under the same excitation conditions. However, future studies will concentrate on the optimization design of the harvester in a wider bandwidth and nonlinear collision modeling. We believe that the results of this study can provide meaningful guidance for designing broadband vibration energy harvesters.

Credit author statement

Bin Zhang: Conceptualization, Methodology, Validation. Haoyuan Li: Investigation, Data curation. Jinhui Liang: Writing - Original Draft, Data Curation, Investigation. Shengxi Zhou: Supervision, Visualization, Validation. Jun Gao: Supervision. Daniil Yurchenko: Writing-Reviewing and Editing, Visualization.

Conflicts of Interest

The author(s) declared no potential conflicts of interest with respect to the research, authorship, and/or publication of this article.

Acknowledgments

This project is supported by the National Natural Science Foundation of China (Grant nos. 51805298, 12072267, 12111530105), the Natural Science Foundation of Shandong Province (Grant no. ZR2019PEE015), the Young Scholars Program of Shandong University, Weihai (Grant no. 20820201004), the Fundamental Research Funds for the Central Universities (Grant no. 2019ZRJC006), and the Royal Society International Exchange 2020 Cost Share (NSFC) program with China IEC\NSFC\201127.

References

[1] Miao G, Fang S, Wang S, Zhou S. A low-frequency rotational electromagnetic energy harvester using a magnetic plucking mechanism. Applied Energy, 2022, 305: 117838. https://doi.org/10.1016/j.apenergy.2021.117838

[2] McKay I S, Wang E N. Thermal pulse energy harvesting. Energy, 2013, 57: 632-640. https://doi.org/10.1016/j.energy.2013.05.045

[3] Tan Y K, Panda S K. Energy harvesting from hybrid indoor ambient light and thermal energy sources for enhanced performance of wireless sensor nodes. IEEE Transactions on Industrial Electronics, 2010, 58(9): 4424-4435. https://ieeexplore.ieee.org/document/5675682/

[4] Yang K, Wang J, Yurchenko D. A double-beam piezo-magneto-elastic wind energy harvester for improving the galloping-based energy harvesting. Applied Physics Letters, 2019, 115(19): 193901. https://doi.org/10.1063/1.5126476

[5] Litak G, Friswell M I, Adhikari S. Magnetopiezoelastic energy harvesting driven by random excitations. Applied Physics Letters, 2010, 96(21): 214103. https://doi.org/10.1063/1.3436553

[6] Al Shami E, Wang Z, Wang X. Non-linear dynamic simulations of two-body wave energy converters via identification of viscous drag coefficients of different shapes of the submerged body based on numerical wave tank CFD simulation. Renewable Energy, 2021. https://doi.org/10.1016/j.renene.2021.07.068

[7] Zhang L, Zhang F, Qin Z, et al. Piezoelectric energy harvester for rolling bearings with capability of self-powered condition monitoring. Energy, 2021: 121770. https://doi.org/10.1016/j.energy.2021.121770

[8] Song R, Shan X, Lv F, et al. A novel piezoelectric energy harvester using the macro fiber composite cantilever with a bicylinder in water. Applied Sciences, 2015, 5(4): 1942-1954. https://doi.org/10.3390/app5041942

[9] Pathak S, Zhang R, Bun K, et al. Development of a novel wind to electrical energy converter of passive ferrofluid levitation through its parameter modelling and optimization. Sustainable Energy Technologies and Assessments, 2021, 48: 101641. https://doi.org/10.1016/j.seta.2021.101641

[10] Hwang W, Kim K B, Cho J Y, et al. Watts-level road-compatible piezoelectric energy harvester for a self-powered temperature monitoring system on an actual roadway. Applied Energy, 2019, 243: 313-320. https://doi.org/10.1016/j.apenergy.2019.03.122

[11] Zhang B, Li D Z, Li Y R, Ducharne B, Gao J. Double Peak Derived from Piezoelectric Coefficient Nonlinearity and Proposal for Self-Powered Systems. Transactions of Nanjing University of Aeronautics and Astronautics, 2018, 35(01):109-115. https://doi.org/10.16356/j.1005-

1120.2018.01.109

[12] Shen H, Qiu J, Balsi M. Vibration damping as a result of piezoelectric energy harvesting. Sensors and Actuators A: Physical, 2011, 169(1): 178-186. https://doi.org/10.1016/j.sna.2011.04.043

[13] Zhang H, Yuan W, Hao Y, et al. Influences of the feedthrough capacitance on the frequency synchronization of the weakly coupled resonators. IEEE Sensors Journal, 2015, 15(11): 6081-6088. https://doi.org/10.1109/JSEN.2015.2453401

[14] Gao M, Wang P, Jiang L, et al. Power generation for wearable systems. Energy & Environmental Science, 2021, 14(4): 2114-2157. https://doi.org/10.1039/D0EE03911J

[15] Liu W, Badel A, Formosa F, et al. A wideband integrated piezoelectric bistable generator: experimental performance evaluation and potential for real environmental vibrations. Journal of Intelligent Material Systems and Structures, 2015, 26(7): 872-877. https://doi.org/10.1177/1045389X14546660

[16] Bao B, Wang Q. A rain energy harvester using a self-release tank. Mechanical Systems and Signal Processing, 2021, 147: 107099. https://doi.org/10.1016/j.ymssp.2020.107099

[17] Bao B, Chen W, Wang Q. A piezoelectric hydro-energy harvester featuring a special container structure. Energy, 2019, 189: 116261. https://doi.org/10.1016/j.energy.2019.116261

[18] Liu Z, Wang X, Al Shami E, et al. A study of a speed amplified linear generator for low-frequency wave energy conversion. Mechanical Systems and Signal Processing, 2021, 149: 107226. https://doi.org/10.1016/j.ymssp.2020.107226

[19] Wu Y, Li S, Fan K, et al. Investigation of an ultra-low frequency piezoelectric energy harvester with high frequency up-conversion factor caused by internal resonance mechanism. Mechanical Systems and Signal Processing, 2022, 162: 108038. https://doi.org/10.1016/j.ymssp.2021.108038

[20] Gu Y, Liu W, Zhao C, et al. A goblet-like non-linear electromagnetic generator for planar multi-directional vibration energy harvesting. Applied Energy, 2020, 266: 114846. https://doi.org/10.1016/j.apenergy.2020.114846

[21] Fan K, Qu H, Wu Y, et al. Design and development of a rotational energy harvester for ultralow frequency vibrations and irregular human motions. Renewable Energy, 2020, 156: 1028-1039. https://doi.org/10.1016/j.renene.2020.04.117

[22] Jia Y. Review of nonlinear vibration energy harvesting: Duffing, bistability, parametric, stochastic and others. Journal of Intelligent Material Systems and Structures, 2020, 31(7): 921-944. https://doi.org/10.1177/1045389X20905989

[23] Ghayesh M H, Farokhi H. Nonlinear broadband performance of energy harvesters. International Journal of Engineering Science, 2020, 147: 103202. https://doi.org/10.1016/j.ijengsci.2019.103202

[24] Mallick D, Amann A, Roy S. Analysis of nonlinear spring arm for improved performance of vibrational energy harvesting devices. Journal of Physics: Conference Series. IOP Publishing, 2013, 476(1): 012088. https://doi.org/10.1088/1742-6596/476/1/012088

[25] Li H, Qin W, Lan C, et al. Dynamics and coherence resonance of tri-stable energy harvesting system. Smart Materials and Structures, 2015, 25(1): 015001. https://doi.org/10.1088/0964-1726/25/1/015001

[26] Deng W, Wang Y. Non-contact magnetically coupled rectilinear-rotary oscillations to exploit low-frequency broadband energy harvesting with frequency up-conversion. Applied Physics Letters, 2016, 109(13): 133903. https://doi.org/10.1063/1.4963786

[27] Meruane V, Pichara K. A broadband vibration-based energy harvester using an array of piezoelectric beams connected by springs. Shock and Vibration, 2016, 2016. https://doi.org/10.1155/2016/9614842

[28] Dechant E, Fedulov F, Fetisov L Y, et al. Bandwidth widening of piezoelectric cantilever Beam Arrays by mass-tip tuning for low-frequency vibration energy harvesting. Applied Sciences, 2017, 7(12): 1324. https://doi.org/10.3390/app7121324

[29] Ferrari M, Ferrari V, Guizzetti M, et al. Piezoelectric multifrequency energy converter for power harvesting in autonomous microsystems. Sensors and Actuators A: Physical, 2008, 142(1): 329-335. https://doi.org/10.1016/j.sna.2007.07.004

[30] Dhote S, Li H, Yang Z. Multi-frequency responses of compliant orthoplanar spring designs for widening the bandwidth of piezoelectric energy harvesters. International Journal of Mechanical Sciences, 2019, 157: 684-691. https://doi.org/10.1016/j.ijmecsci.2019.04.029

[31] Machado L Q, Yurchenko D, Wang J, et al. Multi-dimensional constrained energy optimization of a piezoelectric harvester for E-gadgets. iScience, 2021, 24(7): 102749.

https://doi.org/10.1016/j.isci.2021.102749

[32] Wei C, Jing X. Vibrational energy harvesting by exploring structural benefits and nonlinear characteristics. Communications in Nonlinear Science and Numerical Simulation, 2017, 48: 288-306. https://doi.org/10.1016/j.cnsns.2016.12.026

[33] Cao D X, Leadenham S, Erturk A. Internal resonance for nonlinear vibration energy harvesting. The European Physical Journal Special Topics, 2015, 224(14): 2867-2880. https://doi.org/10.1140/epjst/e2015-02594-4

[34] Zhao L C, Zou H X, Wu Z Y, et al. Dynamically synergistic regulation mechanism for rotation energy harvesting. Mechanical Systems and Signal Processing, 2021: 108637. https://doi.org/10.1016/j.ymssp.2021.108637

[35] Ma X, Li H, Zhou S, et al. Characterizing nonlinear characteristics of asymmetric tristable energy harvesters. Mechanical Systems and Signal Processing, 2022, 168: 108612. https://doi.org/10.1016/j.ymssp.2021.108612

[36] Wei C, Jing X. A comprehensive review on vibration energy harvesting: Modelling and realization. Renewable and Sustainable Energy Reviews, 2017, 74: 1-18. https://doi.org/10.1016/j.rser.2017.01.073

[37] Li M, Jing X. Novel tunable broadband piezoelectric harvesters for ultralow-frequency bridge vibration energy harvesting. Applied Energy, 2019, 255: 113829. https://doi.org/10.1016/j.apenergy.2019.113829

[38] Chen L Q, Jiang W A. Internal resonance energy harvesting. Journal of Applied Mechanics, 2015, 82(3). https://doi.org/10.1115/1.4029606

[39] Lu Z Q, Shao D, Fang Z W, et al. Integrated vibration isolation and energy harvesting via a bistable piezo-composite plate. Journal of Vibration and Control, 2020, 26(9-10): 779-789. https://doi.org/10.1177/1077546319889815

[40] Huang D, Chen J, Zhou S, et al. Response regimes of nonlinear energy harvesters with a resistor-inductor resonant circuit by complexification-averaging method. Science China Technological Sciences, 2021, 64(6): 1212-1227. https://doi.org/10.1007/s11431-020-1780-x

[41] Lu Z Q, Zhao L, Ding H, et al. A dual-functional metamaterial for integrated vibration isolation and energy harvesting. Journal of Sound and Vibration, 2021: 116251.

https://doi.org/10.1016/j.jsv.2021.116251

[42] Zhou S, Zuo L. Nonlinear dynamic analysis of asymmetric tristable energy harvesters for enhanced energy harvesting. Communications in Nonlinear Science and Numerical Simulation, 2018, 61: 271-284. https://doi.org/10.1016/j.cnsns.2018.02.017

[43] Li Z, Liu Y, Yin P, et al. Constituting abrupt magnetic flux density change for power density improvement in electromagnetic energy harvesting. International Journal of Mechanical Sciences, 2021, 198: 106363. https://doi.org/10.1016/j.ijmecsci.2021.106363

[44] Zhou S, Cao J, Inman D J, et al. Impact-induced high-energy orbits of nonlinear energy harvesters. Applied Physics Letters, 2015, 106(9): 093901. https://doi.org/10.1063/1.4913606

[45] Dai H, Wang Y K, Wang L. Nonlinear dynamics of cantilevered microbeams based on modified couple stress theory. International Journal of Engineering Science, 2015, 94: 103-112. https://doi.org/10.1016/j.ijengsci.2015.05.007

[46] Su M, Xu W, Zhang Y, et al. Response of a vibro-impact energy harvesting system with bilateral rigid stoppers under Gaussian white noise. Applied Mathematical Modelling, 2021, 89: 991-1003. https://doi.org/10.1016/j.apm.2020.07.022

[47] Pan P, Qin W Y, Yang Y F, et al. A collision impact based energy harvester using piezoelectric polyline beams with electret coupling. Journal of Physics D: Applied Physics, 2021, 54: 225502 https://doi.org/10.1088/1361-6463/abe968

[48] Zhao D, Wang X, Cheng Y, et al. Analysis of single-degree-of-freedom piezoelectric energy harvester with stopper by incremental harmonic balance method. Materials Research Express, 2018, 5(5): 055502. https://doi.org/10.1088/2053-1591/aabefc

[49] Fang S, Wang S, Miao G, et al. Comprehensive theoretical and experimental investigation of the rotational impact energy harvester with the centrifugal softening effect. Nonlinear Dynamics, 2020, 101(1): 123-152. https://doi.org/10.1007/s11071-020-05732-1

[50] Peng Y, Xu Z, Wang M, et al. Investigation of frequency-up conversion effect on the performance improvement of stack-based piezoelectric generators. Renewable Energy, 2021, 172: 551-563. https://doi.org/10.1016/j.renene.2021.03.064

[51] Soliman M S M, Abdel-Rahman E M, El-Saadany E F, et al. A wideband vibration-based energy harvester. Journal of Micromechanics and Microengineering, 2008, 18(11): 115021.

https://doi.org/10.1088/0960-1317/18/11/115021

[52] Lo C C. A cantilever Beam Chattering against a stop. Journal of Sound and Vibration, 1980, 69(2): 245-255. https://doi.org/10.1016/0022-460X(80)90609-4

[53] Tsai H C, Wu M K. Methods to compute dynamic response of a cantilever with a stop to limit motion. Computers & Structures, 1996, 58(5): 859-867. https://doi.org/10.1016/0045-7949(95)00174-F

[54] Liu H, Lee C, Kobayashi T, et al. Investigation of a MEMS piezoelectric energy harvester system with a frequency-widened-bandwidth mechanism introduced by mechanical stoppers. Smart Materials and Structures, 2012, 21(3): 035005. https://doi.org/10.1088/0964-1726/21/3/035005

[55] Le C P, Halvorsen E, et al. Wideband excitation of an electrostatic vibration energy harvester with power-extracting end-stops. Smart Materials and Structures, 2013, 22(7): 075020. https://doi.org/10.1088/0964-1726/22/7/075020

[56] Fang S, Wang S, Zhou S, et al. Exploiting the advantages of the centrifugal softening effect in rotational impact energy harvesting. Applied Physics Letters, 2020, 116(6): 063903. https://doi.org/10.1063/1.5140060

Declaration of interests

☒The authors declare that they have no known competing financial interests or personal relationships that could have appeared to influence the work reported in this paper.

☐The authors declare the following financial interests/personal relationships which may be considered as potential competing interests: